REPORT DOCUMENTATION PAGE

Form Approved
OMB No. 0704-0188

1. REPORT DATE *(DD-MM-YYYY)*	2. REPORT TYPE	3. DATES COVERED *(From - To)*
31-08-2007	STTR Phase II Final Report	14 Feb. 2005 – 31 Aug. 2007

4. TITLE AND SUBTITLE
Nanomodified Carbon/Carbon Composites for Intermediate Temperature Final Report

5a. CONTRACT NUMBER
FA9550-05-C-0028

5b. GRANT NUMBER

5c. PROGRAM ELEMENT NUMBER

6. AUTHOR(S)
Koo, J. H. (1), Pilato, L. A. (2), and Wissler, G. E. (2)

5d. PROJECT NUMBER

5e. TASK NUMBER

5f. WORK UNIT NUMBER

7. PERFORMING ORGANIZATION NAME(S) AND ADDRESS(ES)

1. University of Texas at Austin, Dept. of Mechanical Engineering, 1 University Station, C2200, Austin, TX 78712-0292

2. KAI, LLC
6402 Needham Lane, Austin, TX 78739

8. PERFORMING ORGANIZATION REPORT NUMBER

9. SPONSORING / MONITORING AGENCY NAME(S) AND ADDRESS(ES)
Dr. Charles Y-C Lee
AFOSR/NA
875 N. Randolph St.
Suite 325, Room 3112
Arlington, VA 22203

10. SPONSOR/MONITOR'S ACRONYM(S)
AFOSR

11. SPONSOR/MONITOR'S REPORT NUMBER(S)

12. DISTRIBUTION / AVAILABILITY STATEMENT

Approved for public release; distribution unlimited

AFRL-SR-AR-TR-08-0050

13. SUPPLEMENTARY NOTES

14. ABSTRACT An improved Carbon/Carbon Composite (CCC) with enhanced thermo-oxidative resistant performance at intermediate temperatures (371 to 650°C) is being developed. A nanophase is introduced into the CCC prior to cure for improved and maintained mechanical strength by preventing oxidation of the CCC. Four material systems based on Lonza PT-15 cyanate ester (CE) resin and selected nanoparticles were chosen to produce prepregs. They were fabricated into composites for carbonization and densification to produce nanomodified CCC using CVI process. Two sets of 30.48- by 30.48 by 0.38-cm NCCC panels were fabricated. Ten material systems based on synthetic AR mesophase pitch and silicon carbide nanoparticles in two groups were also selected to produce CCC using the SMJ patented in-situ polymerization method. Two sets of 15.25 by 15.25 by 0.32-cm CCC panels were fabricated for these two groups. A C/C and a C/SiC type composites fabricated by DACC of Korea were included for comparison. Microstructure analyses of pre- and post-test CCC specimens using SEM and optical microscopy provided more fundamental understanding of material behavior. The nanomodified CE CCC (PT15/30B, PT15/Im and PT15/POSS) are more thermo-oxidative resistant than the baseline CCC (PT15). With TGA for heat soaking in air environment, the DACC C/SiC composite exhibited the best performance and the AR mesophase pitch/SiC impregnated with Ceraset™ exhibited the most thermo-oxidative resistant NCCC. It was followed by the AR mesophase pitch/SiC NCCC. The nanomodified PT-15 CE NCCC is the most unfavorable of the three NCCC groups. The density of the NCCC and the percentage loading of SiC nanoparticles appear to be the most important factors determining the thermo-oxidative properties of NCCC within the same group.

15. SUBJECT TERMS STTR Report, Carbon-Carbon Composite, Thermo-oxidative Resistance, Nanophase, Surface Modified MMT Clay, Nano-Silcon Carbide, POSS, Carbon Nanofiber, Cyanate Ester, TEM, WAXD, Carbonization, Densification

16. SECURITY CLASSIFICATION OF:			17. LIMITATION OF ABSTRACT	18. NUMBER OF PAGES	19a. NAME OF RESPONSIBLE PERSON
a. REPORT	b. ABSTRACT	c. THIS PAGE			Joseph H. Koo, Sc.D.
U	U	U	U	53	19b. TELEPHONE NUMBER *(include area code)* (512) 589-4170

TABLE OF CONTENTS

Section **Page No.**

EXECUTIVE SUMMARY

The major objective of this material program is to develop an improved carbon/carbon (C/C) composite with enhanced thermo-oxidative resistant performance at intermediate temperatures [371° to 650°C (700 ° to 1,200 °F)]. We proposed that a nanophase be introduced into the C/C composites (CCC), prior to cure, to provide improved and maintained mechanical strength by preventing oxidation of the composites. In this research program, we used two resin systems: Lonza low viscosity cyanate ester (CE), PT-15, and Mitsubishi low viscosity synthesized AR mesophase pitch monomer resins; and several types of nanoparticles: chemically modified montmorillonite (MMT) organoclays, polyhedral oligomeric silsesquioxanes (POSS®), carbon nanofibers (CNFs), buckytubes, and nano-silicon carbide (n-SiC) to create new types of nanomodified CCC (NCCC). Wide angle X-ray diffraction (WAXD) and transmission electron microscopy (TEM) were used to determine the degree of dispersion.

The TEM analyses indicated that the MMT nanoclays, POSS®, CNFs, and n-SiC nanoparticles dispersed very well in the cyanate ester resin. Evidence is presented that a nanophase is formed when nanoparticles such as surface treated clay, carbon nanofibers, POSS®, or n-SiC are introduced into cyanate ester resin and n-SiC into the AR mesophase pitch monomer resin.

Four resin/nanoparticle material systems (based on Lonza CE resin) were selected to produce prepregs. The prepregs were fabricated into composites for carbonization and densification to produce nanomodified CCC using CVI process. A set of two of 30.48- by 30.48 by 0.38-cm (12- by 12- by 0.15-inches) NCCC panels were fabricated for this group. Ten resin/particle material systems (based on synthetic AR mesophase pitch) in two groups were also selected to produce CCC using the SMJ proprietary patented in-situ polymerization method. A set of two of 15.25 by 15.25 by 0.32-cm (6- by 6- by 0.125-inches) CCC panels were fabricated for these two groups. Two additional materials, a C/C and a C/SiC type composites fabricated by DACC of Korea, were included for comparison.

Microstructure analyses of pre- and post-test CCC specimens using SEM and optical microscopy provided more fundamental understanding of material behavior. The nanomodified CE CCC (PT15/30B, PT15/Im and PT15/POSS) are more thermo-oxidative resistant than the baseline CCC (PT15). With TGA for heat soaking in air environment, the DACC C/SiC composite exhibited the best performance and the AR mesophase pitch/SiC impregnated with Ceraset™ exhibited the most thermo-oxidative resistant NCCC. It was followed by the AR mesophase pitch/SiC NCCC. The nanomodified PT-15 CE NCCC is the most unfavorable of the three NCCC groups. The density of the NCCC and the percentage loading of SiC nanoparticles appear to be the most important factors determining the thermo-oxidative properties of NCCC within the same group.

1.0 INTRODUCTION

Carbon/carbon composites (CCC) are traditionally designed and optimized for high temperature applications. They have very high temperature capabilities under inert atmospheric conditions, but without oxidation protection, they suffer from thermo-oxidative instability above ~371°C (~700°F) and result in poor mechanical strength. Oxidation protection technologies developed to be used above ~650°C (~1800°F) in thermo-oxidative environments have had limited success. CCC would be ideal materials to extend organic-based material systems beyond the 371°C (700°F) limit if their mechanical strength can be improved and maintained by preventing oxidation of the composite.

The major objective of this material program is to develop a better CCC with enhanced thermo-oxidative resistant performance at intermediate temperatures [371° to 650°C (700° to 1,200°F)]. We proposed that a nanophase be introduced into the CCC, prior to cure, to provide improved and maintained mechanical strength by preventing oxidation of the composites. In this study, we used:

a) *two resin systems*: Lonza low viscosity cyanate esters, PT-15, and Mitsubishi's low viscosity synthesized mesophase pitch monomer system, AR, and

b) *six types of nanoparticles*: chemically modified montmorillonite (MMT) organoclays, carbon nanofibers, polyhedral oligomeric silsesquioxanes (POSS®), nanosilica, nano-silicon carbide (n-SiC), and buckytubes to create new types of nanomodified CCC.

Two additional C/C and C/SiC composites were also included in this study fabricated by DACC of Changwon, Korea for comparison.

The minor objectives of this investigation are to:

a) develop processes to disperse these nanoparticles uniformly in the cyanate esters and the mesophase pitch monomer resin prior to curing,

b) use wide-angle X-ray diffraction (WAXD), transmission electron microscopy (TEM), and scanning electron microscopy (SEM) to characterize polymer nanocomposite microstructures after curing,

c) study the thermal properties and microstructures of these nanomodified CCCs (NCCCs),

d) evaluate the performance (thermo-oxidative resistance) of these materials in the intermediate temperature range [371° to 650°C (700° to 1,200°F)] after carbonization, and

e) develop the process-structure-property-performance relationships of these groups of novel NCCCs.

2. SELECTION OF MATERIALS

2.1 Resin Systems

Two resin systems were selected for the Phase II study. They are Lonza's Primaset® PT-15 cyanate esters and Mitsubishi AR Synthesized mesophase pitch resin systems.

Cyanate Ester (CE) Resin - Polymer system is the most important component of the CCC materials. Lonza Corporation's Primaset PT-30 cyanate ester [1] was selected for the Phase I study [2-4]. This matrix has 65% char yield, less than 0.5% volatiles, no decomposition by-products during curing, and low viscosity (80cP) at 120°C. The chemical structure of PT-30 resin is shown in Figure 2-1. Shivakumar *et al.* [5, 6] used this resin for the fabrication of CCC successfully. A lower molecular weight, PT-15 cyanate ester [7] was used in this Phase II study.

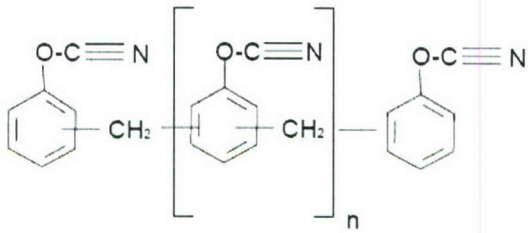

Figure 2-1 Molecular structure of PT-30 cyanate ester resin.

Decomposition of cyanate esters (CE) occurs at about 400-450°C resulting in char (carbon) yields of 63-65% and possibly somewhat higher carbon yields than phenolic (PF) [6, 8]. No gaseous products are emitted on curing CE. Lower volatiles (< 0.5%) are released as compared to volatile solvent (IPA, isopropyl alcohol), water, monomers, etc, being emitted during the pyrolysis of PF. There is economic benefit in using CE instead of PF. Some residual oxygen and nitrogen is retained in the carbonaceous char of the CE. Table 2-1 shows some typical properties of PT-15 CE resin.

Table 2-1 Typical Properties of PT-15 [7]

Properties	**Values**
Appearance	Light yellow liquid (material is waxy at room temperature)
Specific Gravity	1.245
Ionic Cl (ppm)	<10
Ionic Na and K (ppm)	<1
Moisture Content	<0.5
Gel Time at 200°C (min)	>30
Viscosity at 80°C/100°/120°C (cps)	35/15/8
TGA Decomposition Temperature (°C)	420
T_g (°C)	>350

AR Monomer - SMJ Carbon has a proprietary carbon/carbon composite technology based on the use of AR mesophase pitch as well as the polymerization of naphthalene and/or alkyl-naphthalene using a super acid catalyst [9] allowing easy "wet out" of carbon fiber. Synthetic AR [10] possesses a very low softening point and low viscosity at a molten stage while retaining a high coking value and at 100% mesophase. AR is a unique mesophase pitch. When using the mesophase pitch as the matrix of the carbon/carbon composite, the viscosity of the mesophase is a very important factor. If the viscosity is too high, the mesophase pitch does not impregnate

well into carbon fiber perform. There are many advantages in using AR as a raw material of carbon/graphite fibers. The physical properties of the carbon/graphite fiber from AR are far superior to those from conventional mesophase pitches. The carbon fibers from AR show an exception high thermal conductivity. Table 2-2 shows some typical properties of AR.

Table 2-2 Typical Properties of AR [10]

Physical Properties	**Value**	**Solubility (%)**	**Value**
Appearance	Black Pellet	Water Soluble	0
Bulk Density (g/cc)	> 0.65	Benzene Soluble	35 – 44
Specific Gravity (25°C)	1.23	Pyridine Soluble	40 – 50
Specific Heat (cal/g°C)	0.65		
Softening Point (°C) by Mettler	275	Coking Value (%) at 1 hr, 600°C	
Mesophase Content (%)	100	1 atm	80 - 95
Hydrogen/Carbon (atom/atom)	0.58 – 0.64	30 atm	90 - 95
Flash Point (°C)	>300		
Ash (ppm)	<20		

2.2 Polymer Nanoparticles

Several types of nanoparticles were used in this Phase II study. They are listed as follows:

- Surface treated montmorillonite nanoclays (MMT nanoclays) and thermally stable imidazolium-treated layered silicate
- Carbon nanofibers (CNFs)
- Polyhedral oligomeric silsesquioxanes (POSS™)
- Nanosilicas
- Buckytubes (small diameter carbon nanotubes)
- Nano-silicon carbide whiskers and particles

These nanoparticles reinforce the polymer in the nanoscale and enhance the dimensional stability and mechanical properties of the polymer nanocomposites. To achieve the potential improvements nanoparticles usually require some degree of dispersion and exfoliation (for MMT nanoclays). These are shown to be dependent upon a combination of proper chemical treatment and optimized processing. IKA high shear mixing equipment (IKA, Wilmington, NC) was used for dispersing of nanoparticles into CE resin (The IKA unit will be discussed in more detail in the Discussion of Results section).

Montmorillonite Nanoclays - The Cloisite® 30B is an organic surface modified montmorillonite manufactured by Southern Clay Products (SCP) [11]. It is an additive for plastics to improve various plastic physical properties, such as reinforcement, heat distortion temperature, and barrier characteristics. It has ternary ammonium salt modifier at 90 meq/100g clay and is off white in color. Its typical dry particle size and physical properties are shown in Tables 2-3 and 2-4, respectively. Cloisite® 30B in loadings of 5, 10, and 15 wt% were dispersed in a phenolic resole (SC-1008) by Koo *et al.* [12, 13] in rocket ablative application. Enhancement of ablation resistant and insulative properties was noted using phenolic-clay carbon fiber reinforced composite for solid rocket propulsion application.

Table 2-3 Typical Dry Particle Sizes for Cloisite® 30B (Microns, by Volume)

10% LESS THAN	50% LESS THAN	90% LESS THAN
2μ	6μ	13μ

Table 2-4 Physical Properties of Cloisite® 30B(Microns, by Volume)

PROPERTY	CLOISITE® 30B
Loose bulk density, lb/ft^3	14.25
Packed bulk density, lb/ft^3	22.71
Specific gravity	1.98
d_{001}, Å	18.5

In our Phase I study [2-4], PT-15 cyanate ester was blended with several clays (Nanomer® I.28E, Nanomer® I.30E, PWG, Cloisite® 10A, and Cloisite® 30B) using different mixing methods, a total of 34 blends were recorded. Resulting samples were either opaque or translucent. Based on TEM analyses, Cloisite® 30B exhibited the best dispersibility in PT-15 cyanate ester resin and was chosen for this Phase II study.

Introduction of nanoclay by Dean and coworkers [14] increased the onset of non-isothermal decomposition temperature by more than 60°C or greater than 500°C as compared to neat CE. Decomposition of nanomodified CE is shifted to a higher temperature extending CE stability. The effect of nanomodification of CE leads to a multiplicity of mechanical property benefits: higher heat strength, higher modulus, higher fracture toughness, low coefficient of thermal expansion (CTE), and higher T_g.

Newly developed thermally stable imidazolium-treated layered silicates with either Nylon 6 or PET exhibit better stability than commercial nanoclay treated with alkylammonium cations [15]. The use of 1, 2 dimethyl-3-N-alkylimidazolium surface treatment of MMT clay with subsequent intercalation/exfoliation of PET improved the decomposition temperature of the novel imidazolium/MMT clay with PET to a value of 350°C as compared to a value of 250°C for typical quaternary ammonium surface treatment of MMT clay and PET [16]. Recently Dean [17] has examined imidazole surface treated clay and observed improved mechanical, physical properties for Bisphenol A cyanate ester along with improved stability (TGA data).

Substituted imidazolium treated MMT clay systems were examined with PT-15. TGA, TEM and XRD analyses were conducted to compare intercalated/exfoliated PT-15 with imidazolium treated MMT clay and compared with quaternary ammonium surface treated MMT clay and PT-15. Those imidazolium treated MMT clay/PT-15 which exhibit improved TGA behavior vs. quaternary ammonium surface treated MMT clay were combined with PT-15, were coated on T300 fabric, cured, and carbonized for comparison to earlier quaternary ammonium surface treated MMT clay with PT-15.

Carbon Nanofibers (CNF) – CNF are a form of vapor grown carbon fiber, which is a discontinuous graphitic filament produced in the gas phase from the pyrolysis of hydrocarbons

[18-21]. In properties of physical size, performance improvement, and product cost, CNF completes a continuum bounded by carbon black, fullerenes, and single-wall to multi-wall carbon nanotubes on one end and continuous carbon fiber on the other [20]. CNF are able to combine many of the advantages of these other forms of carbon for reinforcement in engineered polymers. The CNF have transport and mechanical properties that approach the theoretical values of single crystal graphite, similar to the fullerenes, but can be made in high volumes at low cost - ultimately lower than conventional carbon fibers. In equivalent production volumes, CNF is projected to have a cost comparable to E-glass on a per-pound basis, yet possess properties which far exceed those of glass and are equal to, or exceed those of much more costly commercial carbon fiber. Maruyama and Alam published an excellent review of carbon nanotubes and nanofibers for use in composite materials [21]. A recent review of the fabrication and properties of CNF in polymer composites was published by Tibbetts et al. [20].

Carbon nanofibers (CNF) are manufactured by Applied Sciences Inc./Pyrograf® Products by pyrolytic decomposition of methane in the presence of iron-based catalyst particles at temperatures above 900°C. Pyrograf®-III is a patented, very fine, highly graphitic, carbon nanofiber. Pyrograf®-III is available in diameters ranging from 65 to 200 nm and a length of 50-100 μm. Therefore, CNF are much smaller than conventional continuous or milled carbon fibers (5-10 μm) but significantly larger than carbon nanotubes (1-10 nm). Compared to PAN and pitch-based carbon fiber, the morphology of CNF is unique in that there are far less impurities in the filament, providing for graphitic and turbostatic graphite structures, and the graphene planes are more preferentially oriented around the axis of the fiber. Consequences of the circumferential orientation of high purity graphene planes are a lack of cross-linking between the graphene layers, and a relative lack of active sites on the fiber surface, making it more resistant to oxidation, and less reactive for bonding to matrix materials. Also in contrast to carbon fiber derived from PAN or pitch precursors, CNF is produced only in a discontinuous form. The length of the CNF can be varied from about 100 μm to several cm, and the diameter is of the order of 100 nm.

Carbon nanofibers have exceptional mechanical and transport properties suggesting excellent potential as an engineering material. Table 2-5 lists the properties of vapor-grown carbon fibers, both as grown, and after a graphitizing heat treatment to 3,000°C. Note that, due to the difficulty of direct measurements on the nanofibers, the values in Table 2-5 are measured on vapor-grown fibers that have been thickened to several microns in diameter [18]. Such fibers consist almost exclusively of CVD carbon, which is less graphitic and more defective than the catalytically grown carbon core that constitutes the carbon nanofiber. Thus the properties listed in the table represent an estimate of the properties of nanofibers.

Table 2-5 Properties of Carbon Nanofibers

Property (Units)	As Grown	Heat Treated
Tensile Strength (GPa)	2.7	7.0
Tensile Modulus (GPa)	400	600
Ultimate Strain (%)	1.5	0.5
Density (g/cc)	1.8	2.1
Electrical Resistivity (μΩ-cm)	1000	55
Thermal Conductivity (W/m-K)	20	1950

The thermal stability of CNF in air was studied in the TGA dynamic heating rate mode by S. Kumar's group [22]. In this mode, to maximize weight change resolution, heating rate was continuously adjusted automatically in response to the changes in the sample's decomposition rate. The heat rate was set as 50°C/min. TGA analyses shows that nanofibers with high oxygen content (PR-24-AG, PR-24-PPO, PR-24-ISO) begin to lose weight just above 300°C, while for fiber containing lower oxygen levels (PR-24-PS and PR-21-PS), the onset of degradation is above 500°C. The onset of degradation for PR-24-HT, which has the least amount of oxygen, is close to 700°C.

In our recent study [23], we examined the thermal stability of several CNFs provided by ASI in a TGA dynamic heating rate mode in the presence of air. The heating rate was initially set at 50°C/min and reduced to 10°C/min in the area of interest. Six CNFs were used namely PR-19-PS, PR-24-PS, PR-19-LHT, PR-24-LHT, PR-19-HHT, and PR-24-HHT. Table 2-6 describes the type of CNFs, diameter, heat treating method, and their decomposition temperatures. Figure 2-2 shows the TGA analyses of these six CNFs. It is evident that the larger diameter PR-19 CNF (150 nm in diameter) has higher thermal stability than the smaller diameter PR-24 CNF (80 nm in diameter) as shown in all three grades. This may due to the higher surface area of PR-24 than PR-19, more surface area results in a faster burning rate. The LHT grade CNF has better thermal stability than the HHT, then followed by the PS grade. The LHT and HHT grades CNF have over 100°C higher decomposition temperatures than the PS grade CNF. The LHT grade has higher stability than the HHT grade for both types of fibers. TEM micrographs show that there are differences in morphology for these two grades. They show that the graphitic structure in HHT grade has areas on the outer surface that may be under high strain which could cause them to thermally degrade at lower temperatures.

Table 2-6 Properties of several CNFs tested by TGA [23]

CNF Type	Diameter (nm)	Heat Treatment Method	Decomposition Temperature (°C)
PR-19-PS	150	Heat stripping the as grown CNF at 400°C to remove any condensed aromatic compounds present on the surface	601
PR-24-PS	80	Same as PR-19-PS	572
PR-19-LHT	150	Heat treating the PR-19 fiber at 1,500°C in an inert atmosphere	742
PR-24-LHT	80	Same as PR-19-LHT	716
PR-19-HHT	150	Heat treating the PR-24 fiber at 3,000°C in a inert atmosphere	730
PR-24-HHT	80	Same as PR-24-HHT	706

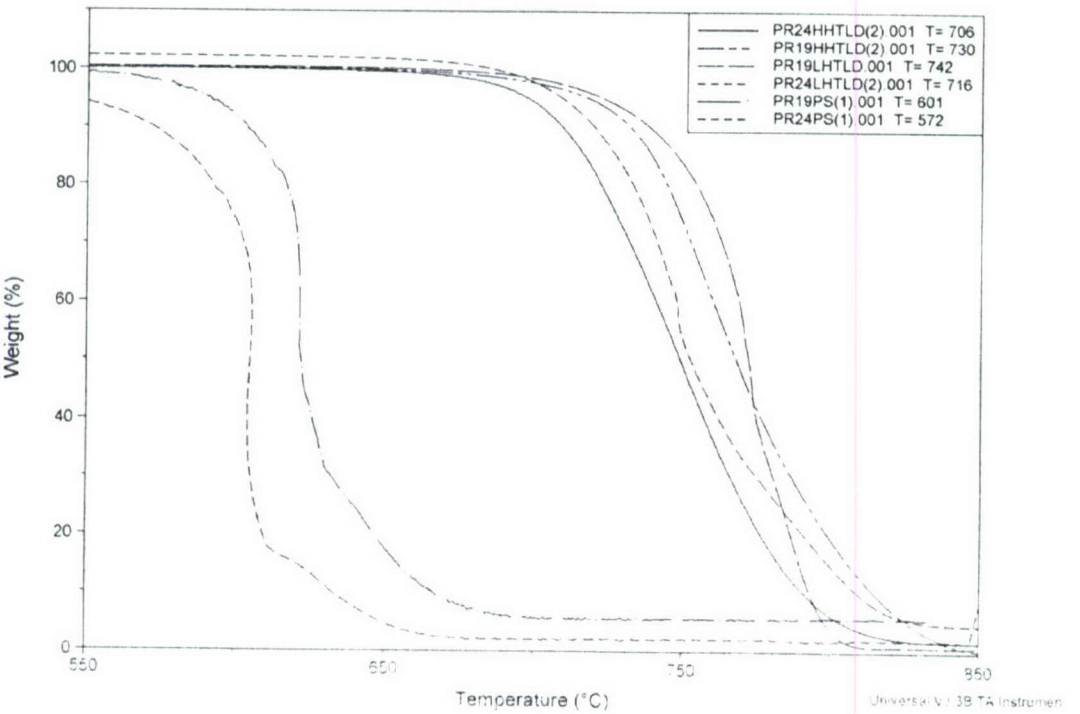

Figure 2-2 TGA of different CNF in air at a heating rate of 50°C/min [23]

Besides differences in structural characteristics of nanomodified CCC, it is anticipated that the pyrolyzed CE/CF modified with CNF should exhibit improved oxidative stability based on the observations of Matsuo [24] who reported enhanced oxidative stabilization of PAN (precursor to CF) and VGCF (a form of CNF) mixture heat treated at 180-350°C in an oxidative atmosphere and transformed into "CNF" modified CF.

POSS® - Representing a merger between chemical and filler technologies, POSS® Nanostructured™ materials can be used as multifunctional polymer additives, acting simultaneously as molecular level reinforcements, processing aids, and flame retardants. POSS® Nanostructured™ materials have two unique structural features: (1) the chemical composition is a hybrid, intermediate ($RSiO_{1.5}$) between that of silica (SiO_2) and silicones (R_2SiO); (2) POSS® molecules are nanoscopic in size, ranging from approximately 1-3 nm. Recommendations of POSS® Materials for ablative applications focus on vinyl-containing POSS® Nanostructured™ materials. These materials can readily form silicon oxycarbide chars that protect the underlying virgin material from degradation. Hybrid Plastics' trisilanolphenyl-POSS® (SO1458) [25] is the material of choice for phenolic and cyanate ester resin systems as shown in Phase I study. Figure 2-3 shows the chemical structure of this POSS® that was also used in Phase II NCCC formulations. POSS®-based NCCCs were studied to determine whether POSS® is a viable nanoparticle component when production volumes for SO1458 are much higher and result in lower price.

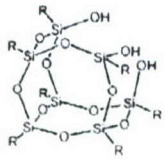

R = phenyl

SO1458
TriSilanolPhenyl-POSS

$C_{42}H_{38}O_{12}Si_7$ MW: 931.34 g/mole

Soluble: tetrahydrofuran, chloroform, ethanol

Insoluble: hexane

Appearance: white powder Refrigerate

Figure 2-3 Chemical structure of trisilanolphenyl-POSS® (SO1458)

Nanosilica – AEROSIL is highly dispersed, amorphous, very pure silica which is produced by high temperature hydrolysis of silicon tetrachloride in an oxyhydrogen gas flame [26-28]. The primary particles are spherical and free of pores. The primary particles in the flame interact to develop aggregates which join together reversibly to form agglomerates. Figure 2-4 shows a TEM micrograph of AEROSIL® 300 in which the primary particles, aggregates and agglomerates can be clearly seen [26]. The average diameters of the primary particles are in the range of 7 to 40 nm according to the AEROSIL grade. The specific surface areas range between 50 to 380 m^2/g. Siloxane and silanol groups are situated on the surface of the AEROSIL particles. The latter is responsible for the hydrophilic behavior of the untreated AEROSIL. Hydrophilic and hydrophobic grades of AEROSIL have proved successful for use in numerous applications such as reinforcing filler, thickening and thixotropic agent, anti-settling agent, and free-flow aid.

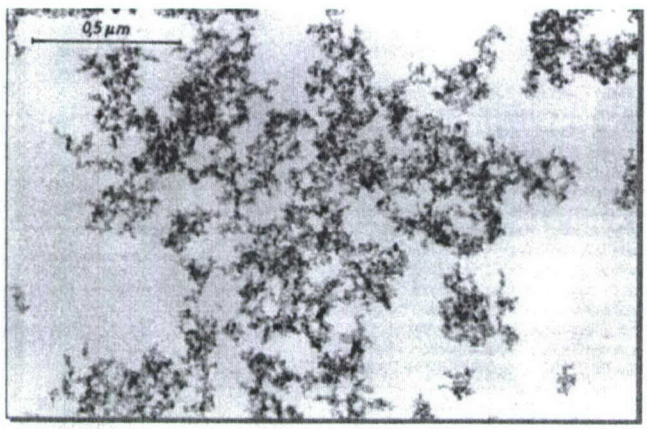

Figure 2-4 TEM micrograph of AEROSIL® 300 [26].

It is also used to adjust the rheological properties of epoxy resins. Two new Degussa products were selected for this investigation such as hydrophobic AEROSIL® R202 and AEROSIL® R805 materials. They also serve as rheological aids to provide effective, stable thickening and thixotropy of epoxy systems [26-28]. Nelson and co-workers used nanosilica with polystyrene in their recent study resulting in significant improvement in reduced flammability [29]. Typical properties of AEROSIL® R805 [27] and R202 [28] are listed in Table 2-7.

Table 2-7 Material Properties of AEROSIL® R805 and R 202 [27, 28]

PROPERTIES	AEROSIL® R 805	AEROSIL® R 202
Specific surface area (BET) (m^2/g)	150 ± 25	100 ± 20
Carbon content (%)	4.5 – 6.5	3.5 – 5.0
Average primary particle size (nm)	12	14
Tapped density standard material (g/l)	50	50
Moisture 2 hours at 105°C	<0.5	<0.5
Ignition loss 2 hours at 1,000°C based on material dried for 2 hours at 105°C	5.0 – 7.0	4.0 – 6.0
pH value in 4% dispersion	3.5 – 5.5	4.0 – 6.0
SiO_2 – content based on ignited material (%)	>99.8	>99.8

Buckytubes - Produced by Carbon Nanotechnologies, Inc. (CNI), buckytubes consist of rolled-up graphite sheets, akin to multiwall nanotubes but with a smaller diameter (less than 3.5 nm). Typically, buckytubes are multi-walled tubes with several walls of thickness. The length ranges from several hundreds of nanometers to several micrometers. Figure 2-5 shows two TEM images of typical buckytubes which are provided by CNI.

Like ordinary carbon nanotubes, buckytubes exhibit higher strength, stiffness, toughness, as well as electrical and thermal conductivity. Buckytubes are thermally stable up to 550°C in air and 1400°C in anaerobic conditions. Additionally, buckytubes can be customized and surface treated. Such functionalization facilitates dispersion by inducing a favorable interface between the resin and the buckytubes. For the purpose of this investigation, buckytubes were not surface treated because untreated buckytubes are claimed by CNI to disperse well in polar resins.

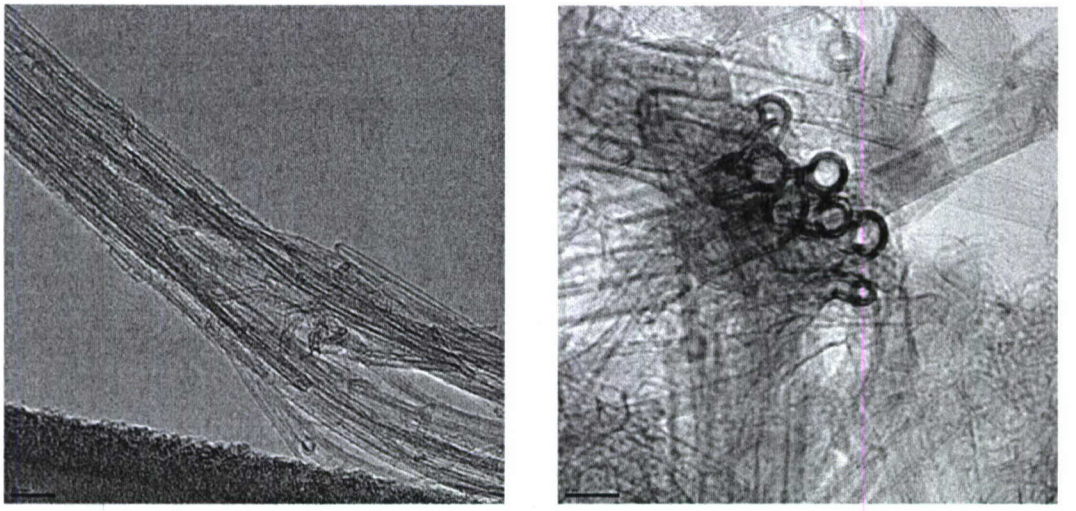

Figure 2-5 High-resolution TEM micrographs of buckytubes in ropes. Scale bar on left is 20nm on the left and 5nm on the right [30, 31].

Nano-Silicon Carbide - Two types of n-SiC from Alpha Materials, Inc. were used such as silicon carbide nanoparticles [32] and nano-silicon carbide crystal whiskers [33]. These nanoparticles will reinforce the polymer binder in the nanoscale and will enhance the dimensional stability and mechanical properties of the resulting carbonized bond by forming a nanophase at the interphase of SiC and the resulting CCC. To achieve these potential improvements, it is necessary to highly disperse these nanoparticles and requires optimized processing.

Nano-Silicon Carbide Particles - Silicon carbide nanoparticles are available from Alpha Materials, Inc. [32]. Nano-SiC particles (*beta* silicon carbide powder) are 50 nm in diameter, >99% purity with a density of 3.21g/cm^3 (Table 2-8). TEM and WAXD of n-SiC are shown in Figures 2-6 and 2-7.

Table 2-8 Properties of SiC Nanoparticles

Property	**Description/Value**
Crystal structure	Cubic
Average particle size	50 nm
Purity	> 99.0%
Si free ions %	0.2%
Cl %	<0.09%
Total oxide %	< 0.61 %
Density	3.21 g/cm^3

Nano crystalline SiC offers the following superior properties:

- Extreme hardness (25-50 GPa bulk and film indentation hardness [34])
- Large semiconductor bandgap (2-3 times larger than silicon [35])
- High electric breakdown field (3-5 times larger than Si [36])
- High thermal conductivity (~390 W/m.K for crystals [37] and ~ 30 W/m.K for SiC fiber/SiC matrix composite [38, 39])
- High specific stiffness (about 3 times larger than Si [40])
- High temperature stability

Silicon carbide nanoparticles were introduced into epoxy resin by Rodgers and coworkers [41] and resulted in improvement in both thermal and mechanical properties of the nanomodified epoxy. Bismaleimide (BMI) resin was nanomodified with SiC nanoparticles (<100nm). The resulting nanomodified BMI exhibited lower friction coefficient and wear loss as well as higher bending and impact strength when compared to neat BMI [42]. The use of n-SiC in these thermosetting resins has been successful in enhancing their respective performance characteristics.

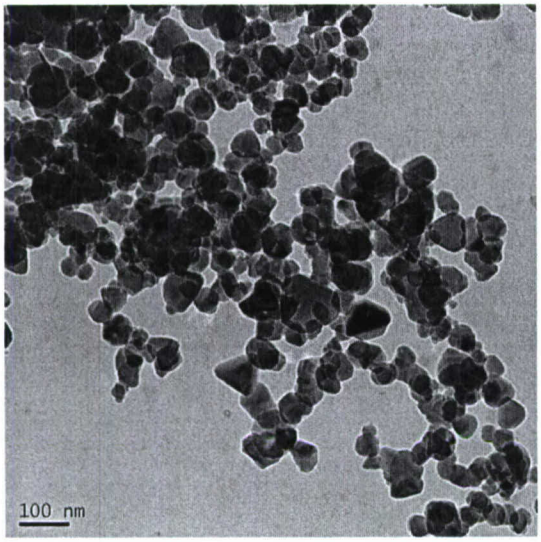

Figure 2-6 TEM of the *beta* SiC powder.

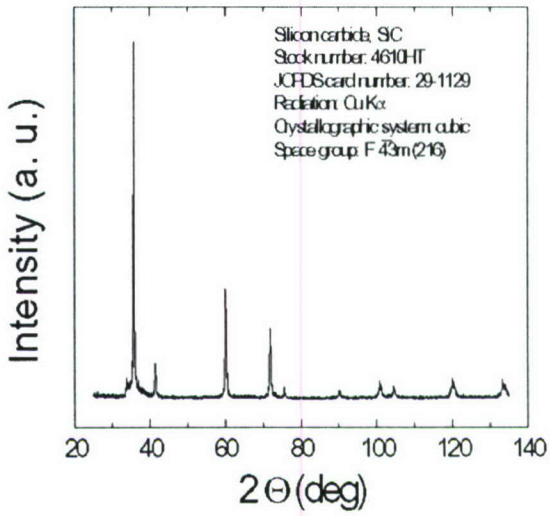

Figure 2-7 X-ray diffraction of *beta* SiC powder.

Nano-Silicon Carbide Crystal Whiskers - Alpha Materials Inc.'s nano-silicon carbide crystal whisker has average diameter of <100 nm with an aspect ratio >10. It's grayish green in color. It has a density of 3.2 g/cc and a high content of SiC of >95%. It has a Moh hardness of 9.5. Figures 2-8 and 2-9 show the SEM and TEM micrographs of the nano-silicon carbide crystal whiskers [33].

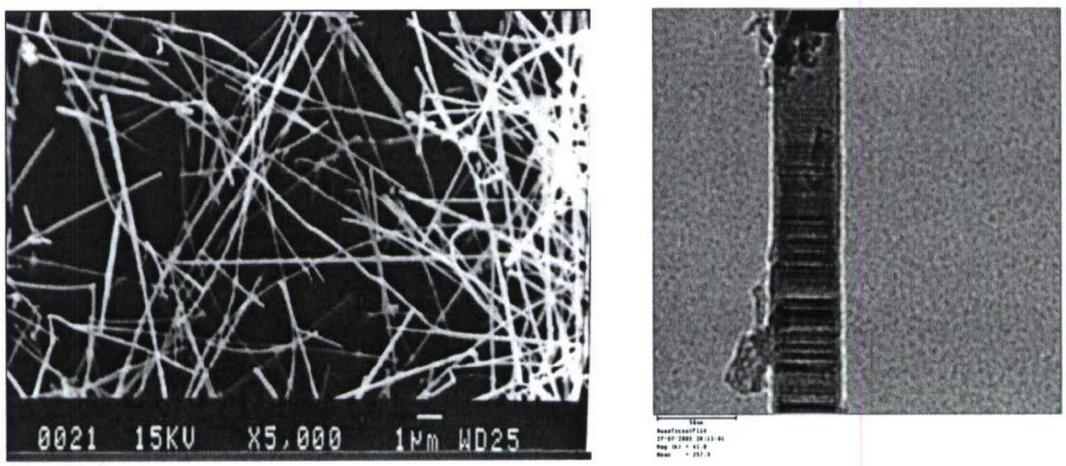

Figures 2-8 and 2-9 SEM (left) and TEM (right, scale bar is 100 nm) micrographs of Alpha Materials' n-silicon carbide crystal whiskers.

Xu *et al.* [43] studied the thermal conductivity effect of SiC whiskers as reinforcement of aluminum matrix composites using an analytical model. The calculated results are in good agreement with experimental data. The dependence of composite thermal conductivity on parameters such as the shape of the SiC reinforcement cluster, the volume fraction inside and outside cluster, has been investigated.

Li *et al.* [44] examined thermally conducting polymer matrix composites containing both aluminum nitride particles and silicon carbide whiskers in a polyimide polymer matrix. Decrease in

coefficient of thermal expansion, increase in thermal conductivity, as well as enhancing the toughness of the composites was reported.

3 MEASUREMENTS

3.1 Morphological Microstructures Analysis

The cross-sections of the PT-15-MMT nanoclay, -POSS, -buckytubes, and -n-SiC nanocomposites were investigated by TEM and SEM to examine the dispersion of the nanoparticles within the PT-15 CE polymer matrix. Uniform distribution of the nanopartcles within the polymer matrix is believed to yield the best enhancement of material properties of the polymer matrix. TEM and SEM are used as screening tools in selecting potential formulations for further testing and characterizations.

3.2 Thermal Stability Testing

Thermal stability of the PT-15 cyanate ester baseline and cyanate ester-buckytubes and cyanate ester-n-SiC nanocomposites were examined by thermogravimetric analysis (TGA) using the Perkin Elmer TGA 7. Weight changes in sample materials are measured as a function of temperature or time in TGA. The sample is heated by a furnace under air while the loss or gain of sample weight due to chemical reactions, decomposition, solvent or water evaporation. Curie point transitions and oxidation are monitored by a sensitive balance. Weight, temperature, and furnace calibrations were carried out within the usable range of the TGA (100-900°C) at scan rates of 5°C/min, 10°C/min, and 20°C/min, respectively.

3.3 Glass Transition Temperature

Differential Scanning Calorimetry is used to measure the glass transition temperature (T_g). Perkin Elmer DSC 7 was used in this investigation. The difference in the amount of heat required to increase the temperature of the sample and the reference are measured as a function of temperature. The characterization temperature range is 50°C to 400°C under air, and at three different heating rates: 5°C/min, 10°C/min, and 20°C/min.

3.4 Thermo-oxidative Studies of NCCC Samples

Two types of heat-aged tests were used to determine the thermo-oxidative resistance of the nanomodified CCCs. All NCCCs were heated at 650°C for 100 hrs using a vacuum furnace. All materials were also heated to 900°C using TGA in air. Airflow rate of 200 cc/min at heating rate of 20°C/min were used for the TGA experiments. Two types of TGA analyses were conducted: (a) Materials were exposed from room temperature (RT) to 900°C (dynamic measurement) with heating rate of 20°C/min and air purging rate at 200 cc/min and (b) Materials were soaking at 650°C with heat rating of 20°C/min and air purging rate at 200 cc/min for 5 hrs.

4. DISCUSSION OF RESULTS

The candidate materials developed are screened for uniformity of dispersion using WAXD and TEM prior to scale up processing. The morphology of selective resin/nanoparticle systems were characterized using TEM and SEM analyses. Three of the nanoparticles such as nanosilica, carbon nanofibers, and buckytubes were eliminated in the polymer-nanoparticle characterization stage due to their poor dispersions in the PT-15 CE resin. As a result, only three types of nanoparticles including nanoclays, POSS, and n-SiC were carried to the CCC fabrication stage.

Detailed processing and characterization of PT-15 CE with nanoclays, POSS, buckytubes, and n-SiC as well as NCCC fabrication and thermo-oxidative studies are included in this section.

Processing - The IKA colloid mixer is a Labor-Pilot 2000/4 module, serial number 1049+. It is designed in the same way as the larger production machines of the 2000 series, and all elements can be transferred to larger machines. This enables an optimum scale-up to production plants. Figure 4-1 shows the recycling batch apparatus for the IKA colloid mixer.

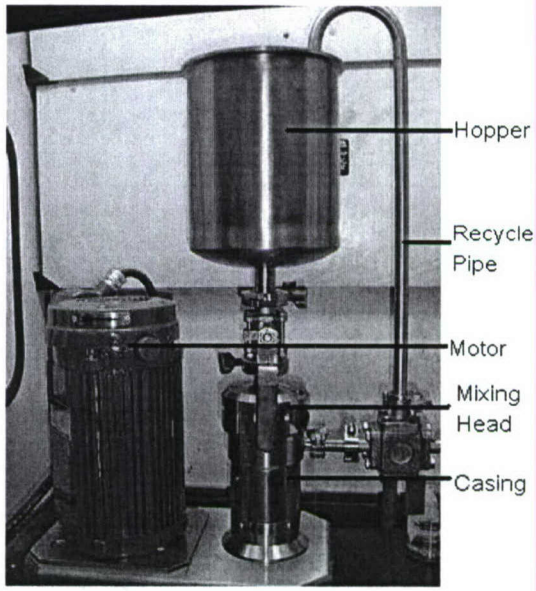

Figure 4-1 Experimental setup of IKA colloid mixer.

The colloid mill is a single-stage high-performance instrument (Ultra-Turrax® Inline) for continuous dispersion of liquids. Originally designed for aqueous systems, the colloid mill can also be used for systems with limited viscosity. The upper temperature tolerance of the system is listed at 120°C. To ensure that viscous polymer does not polymerize, processing temperature can be maintained below 90° with cooling.

Polymer resin is first heated to processing temperature and transferred into hopper, and the rotary shaft generates a sufficient pressure head to pump the polymer through the recycling pipes back to the hopper. This creates a continuously recycling batch production, so long as the material retains a sufficiently low viscosity to recycle. The colloid mill rotor-stator can be fitted with different modules and adapt different fine-toothed generators. For purpose of dispersing nanotubes within cyanate ester, the MK generator module is used and fitted. With a power controller, the operating speed of the IKA mixer can be adjusted from 3,160rpm to 13,750rpm. However, the suggested maximum operational speed is 7,900rpm. For PT-15 cyanate ester, the shaft speed is typically maintained at 5,000rpm or higher to ensure a sufficiently high temperature and shear rate, which is determined by the grinding gap and shaft speed. Experiments show that the maximum gap distance is about 0.5mm. For purpose of generating the highest amount of shear for optimal dispersion, a 0.25mm minimal grinding gap is used.

Typically, the polymer is heated initially to an elevated temperature to attain a processing viscosity; and depending on the formulation, nanoparticles are either premixed in the batch, or added into a continuous system after the neat resin system is circulating and has attained a

steady-state. Generally the former premixing method is used for systems with high nanoparticle weight loading. Since a large scale of dispersion likely increases the polymer viscosity drastically, it is prudent to premix and heat up the entire batch to attain a higher initial temperature and facilitate the initial equilibrium (i.e. ensuring the system runs and recirculates initially, and does not clog up before a steady state is reached). For lower nanoparticle weight loadings, the system does not exhibit a significant increase in viscosity, and can likely equilibrate itself easily. In this scenario, the neat system is first put into recirculation and the nanoparticles added later. This method allows pre-swelling of nanoparticles, as well as close monitoring of material flow and conditions, which simplifies processing. Some processing parameters for neat PT-15 cyanate ester are listed in Table 4-1.

Table 4-1 Processing Parameters for Neat PT-15 Cyanate Ester

Power Input (Shaft Speed)	50Hz (6,500rpm)
Batch Volume	875mL
Initial Temperature	57°C
Quasi-Steady-State Temperature	63°C
Grinding Gap	0.25mm

4.1 Processing and Characterization of PT-15/Nanoclay Systems

In our Phase I study [2-4], PT-15 cyanate ester was blended with several clays (Nanomer® I.28E, Nanomer® I.30E, PWG, Cloisite® 10A, and Cloisite® 30B) using different mixing methods, a total of 34 blends were recorded. Resulting samples were either opaque or translucent.

PT-15/30B (97.5/2.5) THF, PT-15/10A (97.5/2.5) THF, and PT-15/I.30E (97.5/2.5) THF blends were prepared using THF as a carrier medium in these samples to facilitate clay dispersion. All three clays show uniform dispersion as shown in Figures 4-2 through 4-4. When Cloisite® 30B, Cloisite® 10A, and Nanomer® I.30E were compared in higher magnification TEM micrographs, Cloisite® 30B is dispersed slightly more uniformly than the other two clays as shown in Figure 4-2. Cloisite® 30B is in a partial exfoliated state in PT-15 as shown in Figure 4-5. Small tactoids are also present in this nanodispersion. Cloisite® 30B is the preferred clay for the PT-15 resin and for continued study in Phase II.

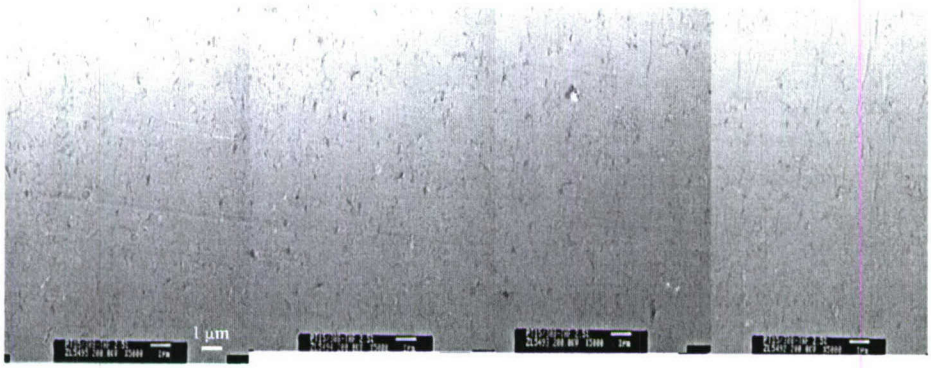

Figure 4-2 TEM micrographs of PT-15/Cloisite® 30B (97.5/2.5) THF showing uniform dispersion of Cloisite® 30B in the PT-15 cyanate ester where scale bar is 1 µm.

Figure 4-3 TEM micrographs of PT-15/Cloisite® 10A (97.5/2.5) THF showing uniform dispersion of Cloisite® 10A in PT-15 cyanate ester where scale bar is 1 µm.

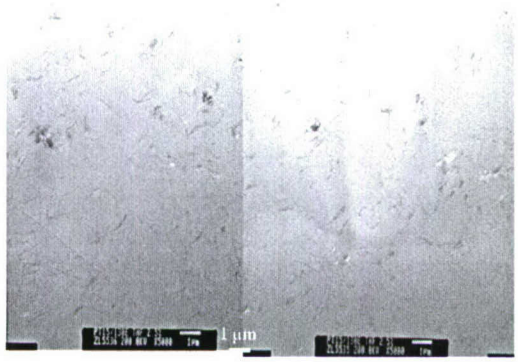

Figure 4-4 TEM micrographs of PT-15/Nanomer® I.30E (97.5/2.5) THF showing uniform dispersion of Nanomer® I.30E in PT-15 cyanate ester where scale bar is 1 µm.

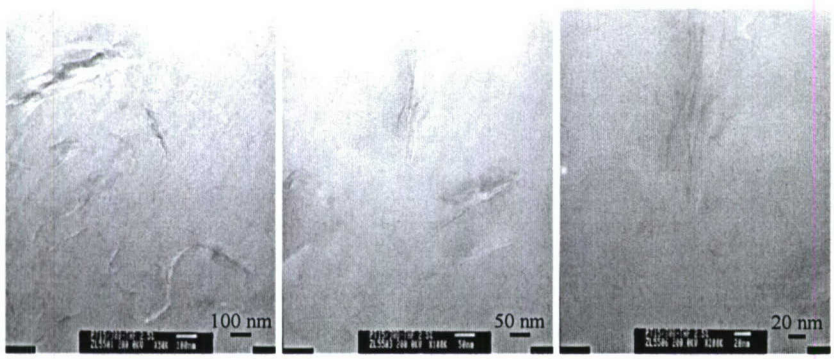

Figure 4-5 Higher magnification TEM micrographs of PT-15/Cloisite® 30B (97.5/2.5) THF showing Cloisite® 30B clays are exfoliated in PT-15 cyanate ester.

Summary and Conclusions – TEM analysis has been demonstrated as an effective tool to characterize and screen candidates based on their degree of dispersion. SCP's Cloisite® 30B

was selected to incorporate into PT-15 CE resin with T-300 3K carbon fabric to produce prepregs and cured composites. A set of two 12- by 12-by 0.15-inches NCCC panels was fabricated using the CVI process as described in Section 4.6.

4.2 Processing and Characterization of PT-15/POSS System

PT-15 was blended with trisilanolphenyl-POSS® in different wt% as well as other POSS materials. A total of 13 blends were recorded in the Phase I study [2-4]. Only PT-15/trisilanolphenyl-POSS® in (99/1) and (97/3) blends were completely transparent. TEMs of PT-15 (pure), SO1458 POSS® (trisilanolphenyl-POSS®), PT-15/SO1458 (97/3), & PT-15/SO1458 (95/5) blends are shown in Figures 4-5 through 4-9. Figure 4-5 shows the TEM of the neat PT-15 resin. The SO1458 POSS® are micron-sized particles in IPA solvent as shown in Figure 4-6. Figures 4-7 and 4-8 show molecular dispersion of SO1458 POSS® in the PT-15/SO1458 (97/3) system. Where particles are noted, one finds their Si content is higher than in the open resin matrix. Significant Si is detected in the resin matrix in regions where no particles are observed. Clearly, the POSS® is partially dissolved in the matrix and partially nanodispersed. SO1458 is a good candidate system for a conversion to CCC. Figure 4-9 shows similar molecular dispersion of SO1458 POSS® in the PT-15/SO1458 (95/5) system. SO1458 POSS® is the preferred POSS® system for the PT-15 resin and retained for Phase II study.

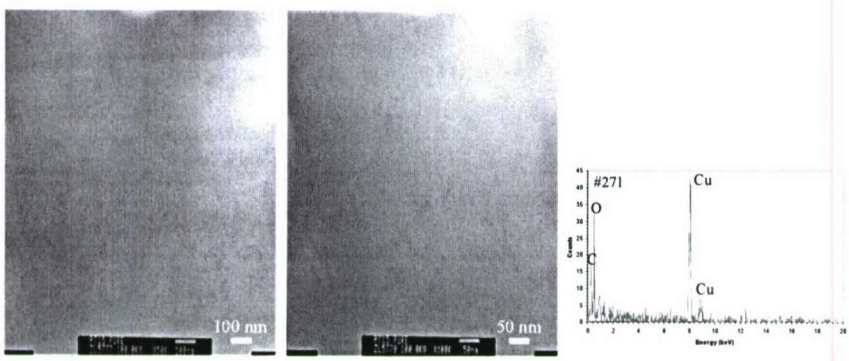

Figure 4-6 TEM micrographs of a neat PT-15 cyanate ester resin.

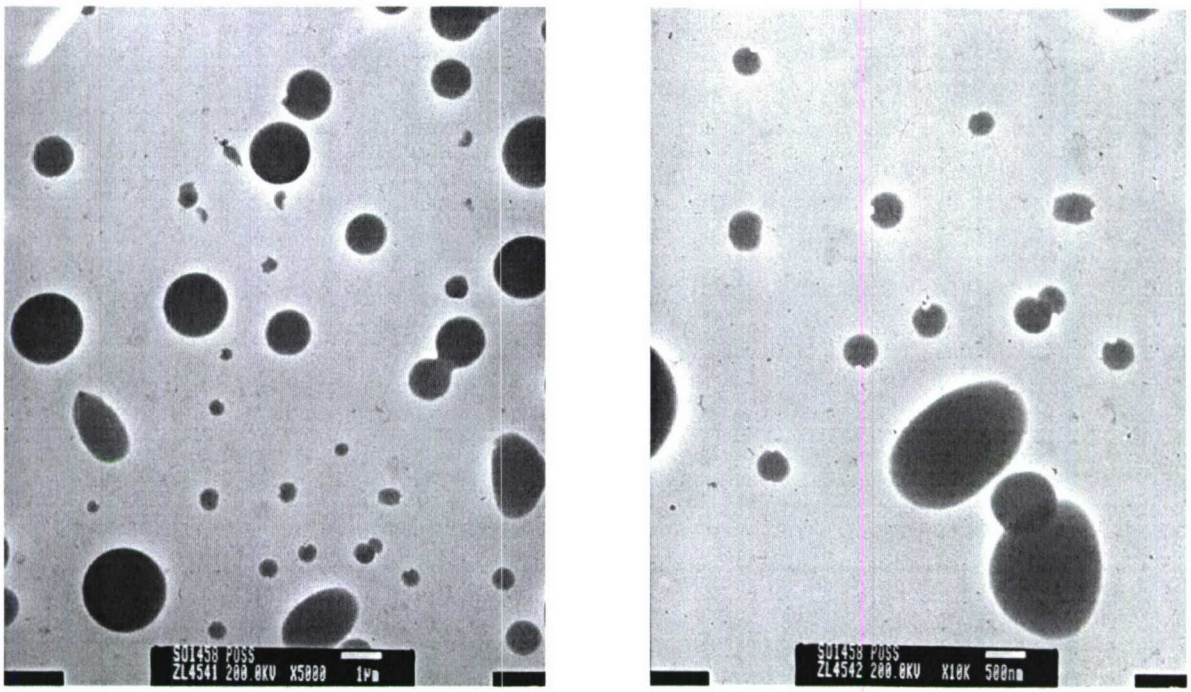

Figure 4-7 TEM micrographs of micron-sized SO1458 POSS® (trisilanolphenyl-POSS®) particles in an IPA solvent where scale bar is 1μm (left) and scale bar is 500 nm (right).

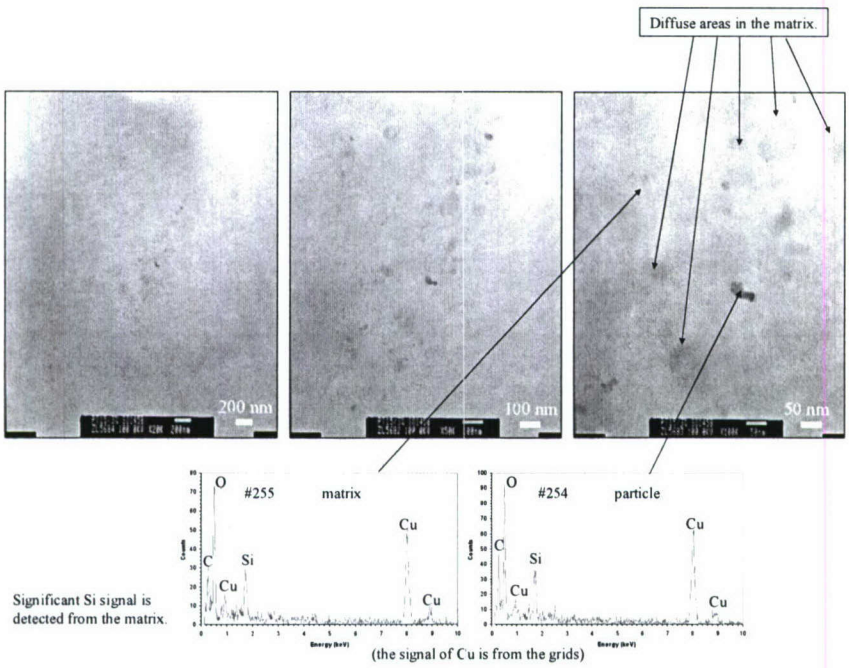

Figure 4-8 Progressive magnification TEM micrographs of PT-15/SO1458 POSS® (97/3) showing molecular dispersion of SO1458 POSS® in PT-15 cyanate ester. Si from POSS® molecules is dispersed in the resin matrix. The dark particle has the same Si/O/C composition as the resin matrix.

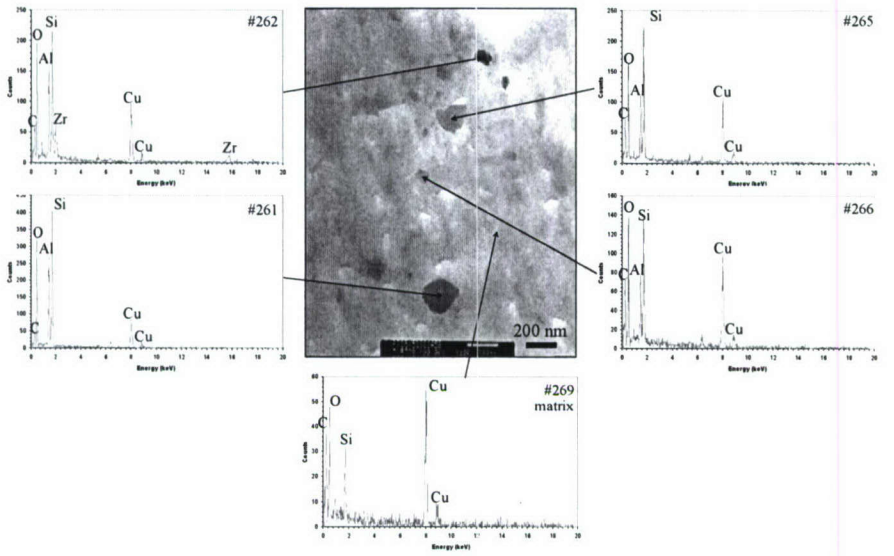

Figure 4-9 Higher magnification TEM micrographs of PT-15/SO1458 POSS® (97/3) showing molecular dispersion of SO1458 POSS® particles in PT-15 cyanate ester. Si is dispersed in the resin matrix. The particles have more Si content than resin.

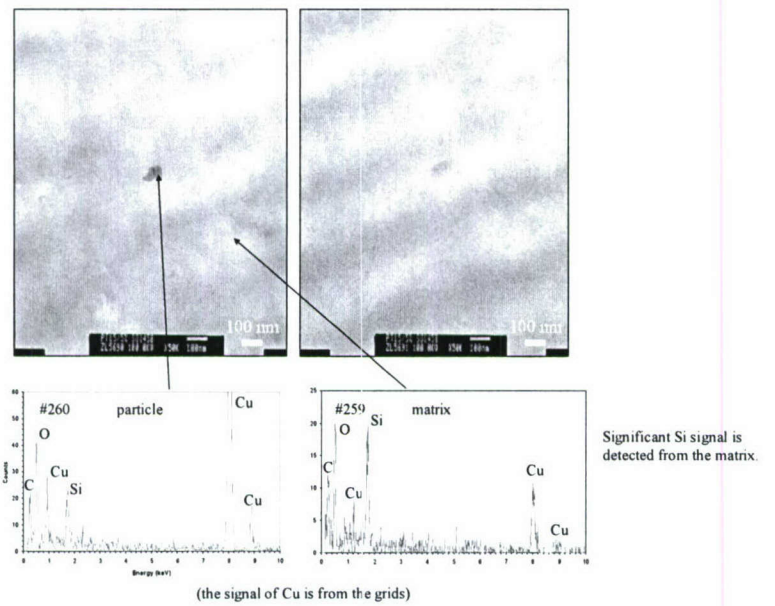

Figure 4-10 TEM micrographs of PT-15/SO1458 POSS (95/5) in high magnification showing molecular dispersion of SO1458 POSS molecules in PT-15 cyanate ester. Significant Si is detected in the resin matrix.

Summary and Conclusions – TEM analysis has been demonstrated as an effective tool to characterize and screen candidates based on their degree of dispersion. Hybrid Plastics' SO1458 POSS® was selected to incorporate into PT-15 CE resin with T-300 3K carbon fabric to produce prepregs and cured composites. A set of two 12- by 12-by 0.15-inches NCCC panels was fabricated using the CVI process as described in Section 4.6.

4.3 Processing and Characterization of PT-15/N-SiC Systems [45]

Several loadings of n-SiC particles were blended into the PT-15 CE resin using high shear mixer. Figures 4-11 and 4-12 show the TEM micrographs of PT15-5% SiC particles nanocomposite and PT15-10% SiC particles nanocomposite, respectively. They show that the SiC nanoparticles were well dispersed in the PT-15 matrix. Figure 4-13 shows the progressive magnification of the TEM micrographs of PT15-10% SiC particle nanocomposite.

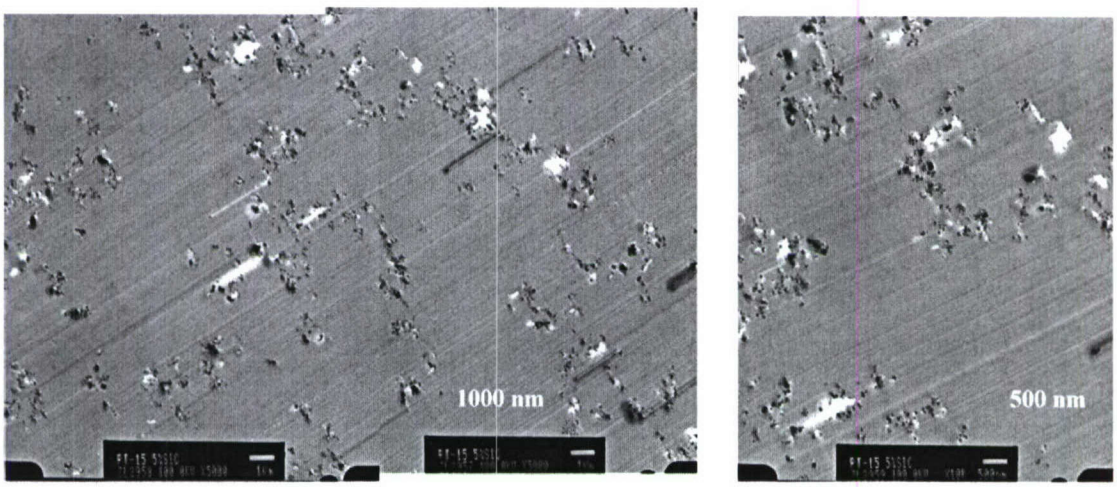

Figure 4-11 TEM micrographs of PT15-5% SiC particles nanocomposite.

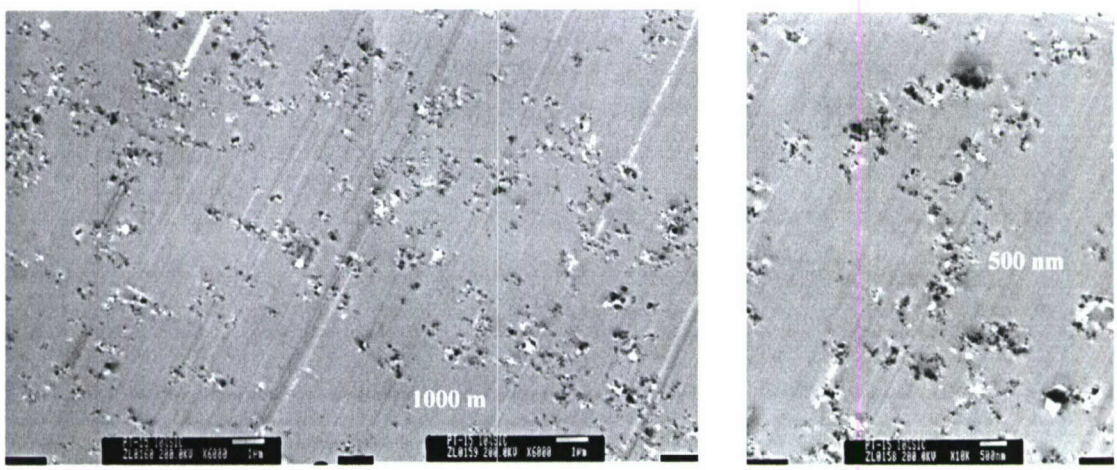

Figure 4-12 TEM micrographs of PT15-10% SiC particles nanocomposite.

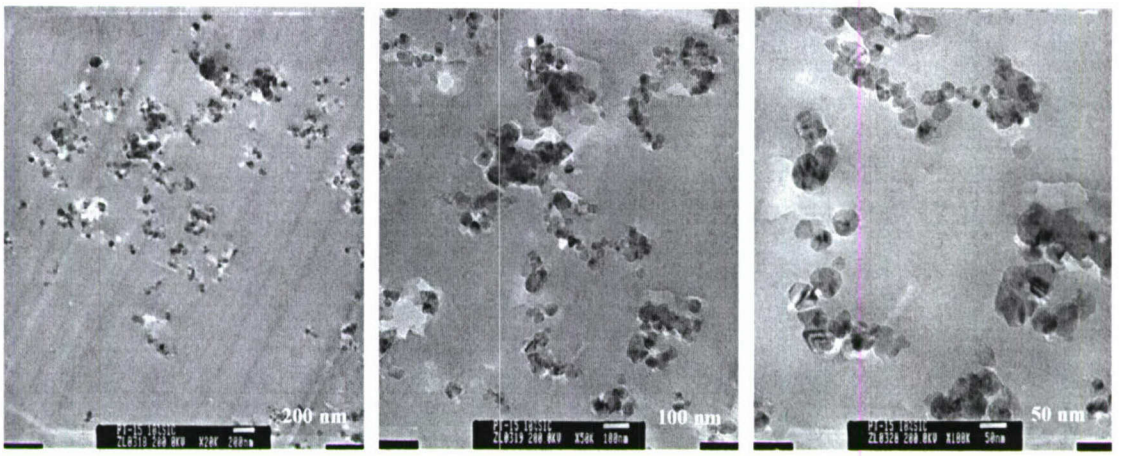

Figure 4-13 TEM micrographs showing progressive magnification of PT15-10% SiC particle nanoparticles.

Figures 4-14 and 4-15 show the TEM micrographs of PT15-5% SiC whisker nanocomposite and PT15-10% SiC whisker nanocomposite, respectively. The n-SiC whiskers didn't disperse well in the PT-15 CE resin, they formed large aggregates.

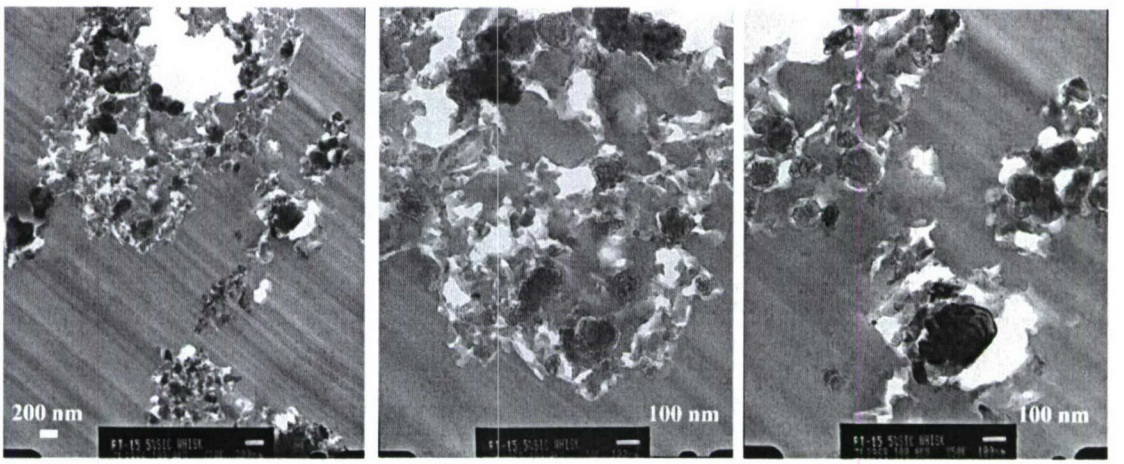

Figure 4-14 TEM micrographs of PT15-5% SiC whisker nanocomposite.

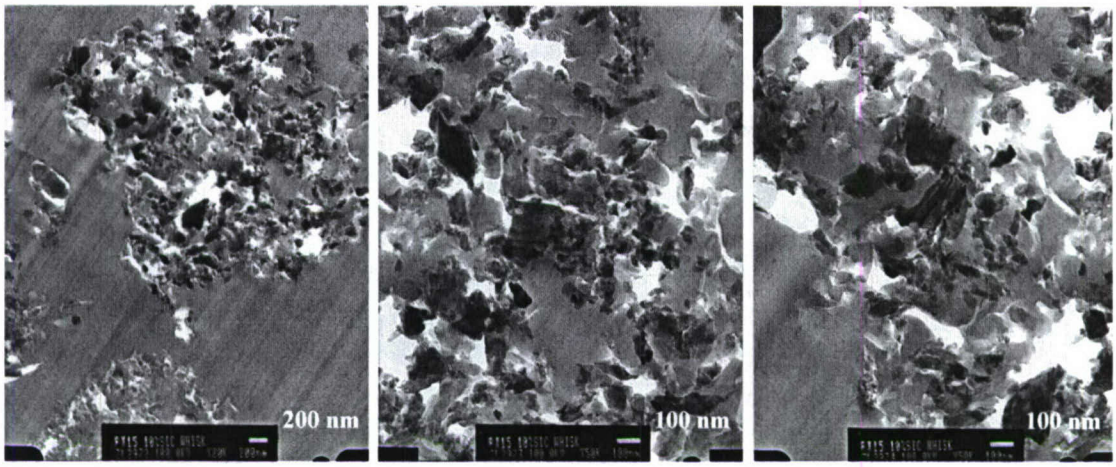

Figure 4-15 TEM micrographs of PT15-10% SiC whisker nanocomposite.

Thermal Stability of PT-15/SiC Systems - Figures 4-16 and 4-17 show the thermogravimetric analysis (TGA) of the PT-15 and the PT15-SiC particles nanocomposites at the scan rate of 10°C/min and 20°C/min, respectively. The change of sample weight was measured as a function of temperature. The decomposition temperatures of the composites with 2%, 5% and 10% SiC nanoparticles were observed to be higher than that of the neat PT-15 material, in which 10% SiC nanoparticles loading level gave the best enhancement on thermal stability. On the other hand, the nanocomposite with 22% SiC particles impaired the thermal stability of the resin system. This indicates that that loading level is excessive for this resin system and that 10%, or an intermediate amount between 10% and 22%, is the optimal loading level of SiC nanoparticles for this PT-15 resin system. This observation needs further investigation of this resin/nanoparticle system.

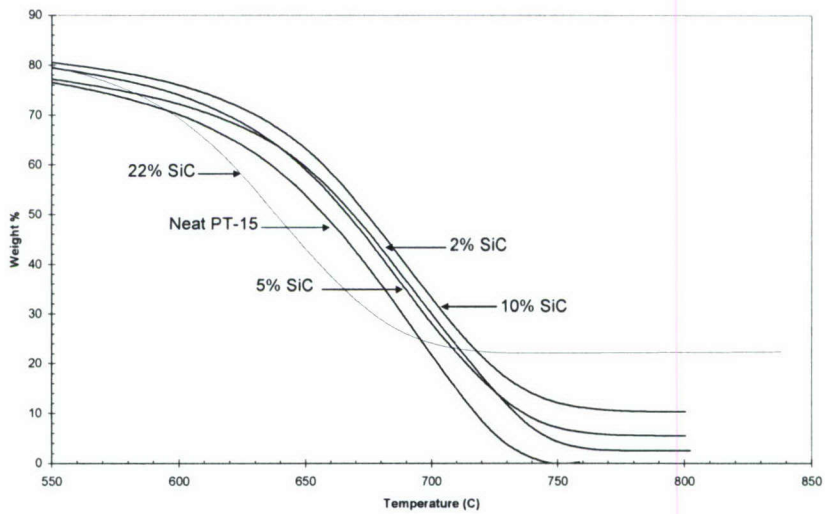

Figure 4-16 Thermogravimetric analysis of PT15-SiC particles nanocomposites at scan rate of 10°C/min.

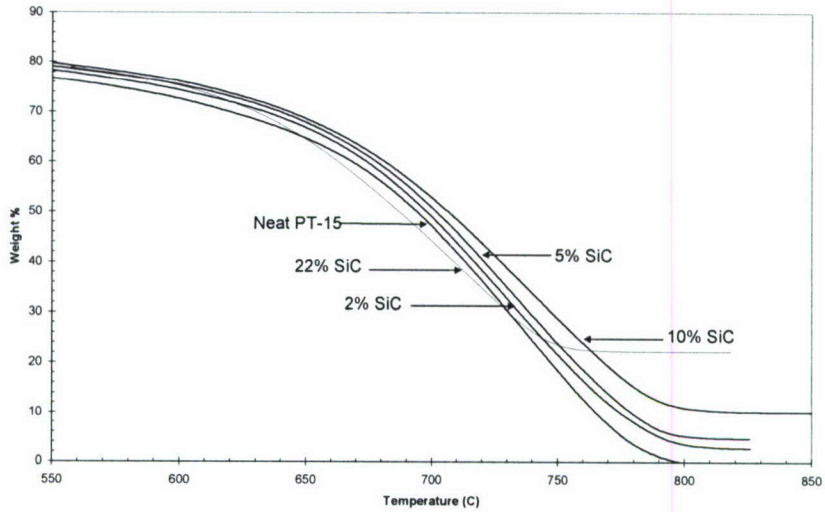

Figure 4-17 Thermogravimetric analysis of PT15-SiC particles nanocomposites at scan rate of 20°C/min.

Figures 4-18 and 4-19 show the thermogravimetric analysis (TGA) of the PT-15 and the PT15-SiC whiskers nanocomposites at the scan rate of 10°C/min and 20°C/min, respectively. The change of sample weight was measured as a function of temperature. The decomposition temperatures of the composites with 2%, and 10% SiC nanoparticles were observed to be about the same as that of the neat PT-15 material. The 5% SiC nanoparticles loading level is less thermal stable than the neat PT-15 material.

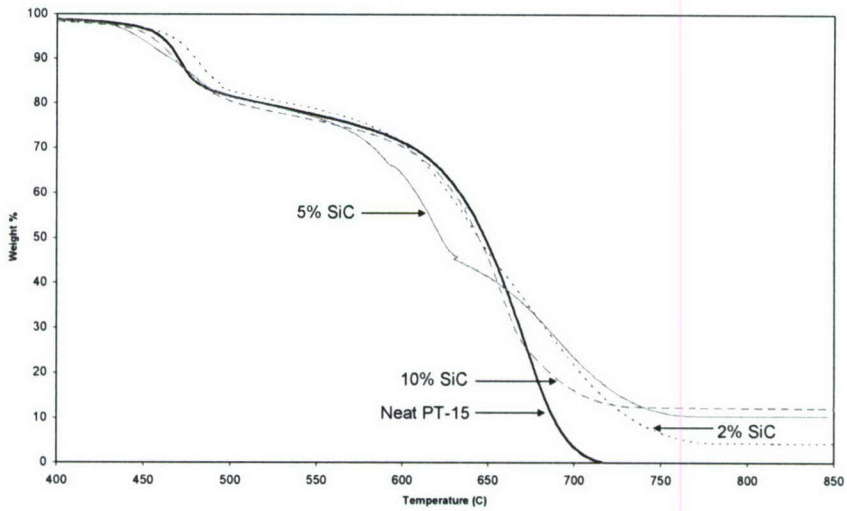

Figure 4-18 Thermogravimetric analysis of PT15-SiC whiskers nanocomposites at scan rate of 10°C/min.

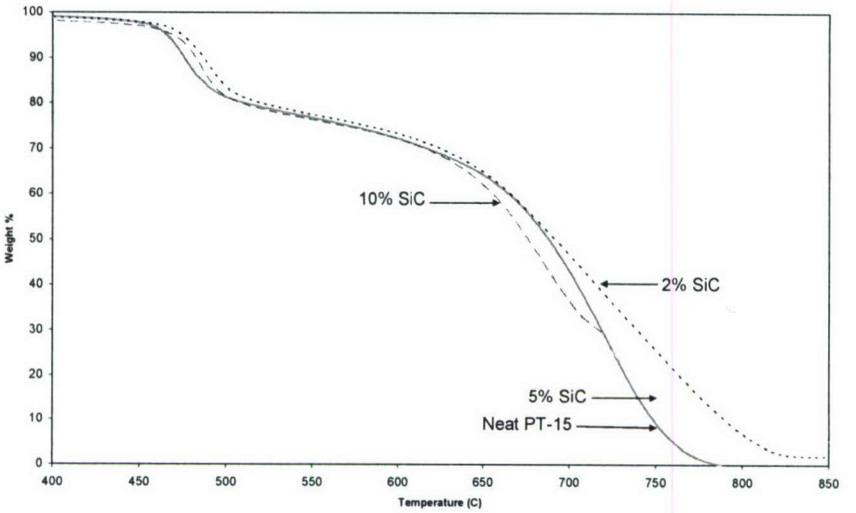

Figure 4-19 Thermogravimetric analysis of PT15-SiC whiskers nanocomposites at scan rate of 20°C/min.

Summary and Conclusions - In summary, the morphological microstructures and thermal stability of the PT-15 with 0, 2%, 5%, 10%, and 22% n-SiC particles resin systems were investigated. The morphological microstructures and thermal stability of the PT-15 with 2%, 5%, and 10% n-SiC whiskers resin systems were also examined. The following conclusions are drawn from this study:

1. All levels (2 %, 5%, 10%) of n-SiC particles were shown to be dispersed well in the PT-15 CE resin as shown by TEM analyses.
2. The n-SiC whisker didn't disperse well in the PT-15 CE resin as shown by the TEM analyses.
3. The decomposition temperatures of the PT-15 CE with 2%, 5%, and 10% n-SiC particles were observed to be higher than that of the PT-15 CE material.
4. The 10% n-SiC particles loading gave the best enhancement on thermal stability, while the 22% n-SiC particle sample harmed the thermal stability of the PT-15 CE resin system. This indicates that the optimal loading is in between 10% and 22% of n-SiC particle for the PT-15 CE resin system.
5. The decomposition temperatures of the 2% and 10% n-SiC whiskers were observed about the same as that of the neat PT-15 CE material. The 5% n-SiC whiskers specimen is less thermally stable than the neat PT-15 CE resin and due to poor dispersion.

4.5 Processing and Characterization of PT-15/Buckytubes Systems [46]

Processing - For processing of PT-15 cyanate ester with buckytubes different conditions such as pre-swelling of buckytubes and monitoring of material flow/conditions were required. For PT-15-1% buckytube formulation, buckytube is first swollen in acetone and then mixed into a running system of PT-15. This processing protocol was used for this portion of the study, as well as many other related research investigations, and had proven effective in attaining a

uniform recirculation. Processing conditions for PT-15/buckytube nanocomposites are listed in Table 4-2.

Table 4-2 Processing Parameters for PT-15/ 1%, 3%, and 5% Buckytubes Nanocomposites

PT-15 Volume & Mass (at room T)	700mL, 735g	760mL, 798g	800mL, 840g
Buckytube mass	7.4g	23.94 g	43.0g
Buckytube wt%	1%	3%	5%
Procedure	Buckytube added after circulating neat PT-15	Buckytube & PT-15 premixed and preheated	Buckytube added after circulating neat PT-15
Power Input (Shaft Speed)	52Hz (6,800rpm)	52Hz (6,800rpm)	60Hz (7,900rpm)
Shear Rate	78,330 s^{-1}	78,330 s^{-1}	91,000 s^{-1}
Initial Temperature	52°C	59°C	58°C
Quasi-Steady State Temperature	68°C	76°C	75°C
Grinding Gap	0.25mm	0.25mm	0.25mm
Mixing Time	42min	46min	16min, aborted due to clogging

Processing and Microstructural Analyses ofPT-15/Buckytube Systems - It is observed that for neat system, the PT-15 undergoes a color change from maple orange-red to opaque oak beige. Upon reheating the processed PT-15, there is significant bubbling and the color changes back to the original maple orange. This is indicative that a very high content of air is suspended in the viscous system. It is speculated that the higher the viscosity of the polymer, the more severe this phenomenon is, because of the inability to evolve through the viscous medium. A degassing procedure was employed after mixing to minimize the air bubbles. The nanocomposite mixture is vacuum heated at 80°C, at which the polymer viscosity decreases drastically. (For reference, neat PT-15 has a viscosity of 35cps at 80°C). The air/volatiles can be removed by vacuum.

For 1wt%buckytube/PT-15, the degassing is very effective. But for 3wt%buckytube/PT-15 and 5wt%buckytube/PT-15, it is evident that the viscosity of the mixtures remains tar-like up to their curing temperature. And thus degassing was not thoroughly successful. Voids are expected in the cured products. For 1wt% buckytube processing, steady-state shaft speed can be tuned to as low as 40Hz (~5,000rpm). Supposedly, lower shear rate incurs less damage to nanotubes and fibers. However, low shear rate also reduces viscosity inherently (PT-15 shear-thinning) as well as decreasing the temperature (at 40Hz, temperature goes down to 50°C), presenting a processing problem. Thus, for ease of processing, the shaft speed is typically maintained at 52Hz and above.

A convection oven is used to cure the mixtures, and specimens are oven cooled. No post-cure heat treatment is applied. Curing cycle used is shown in Figure 4-20.

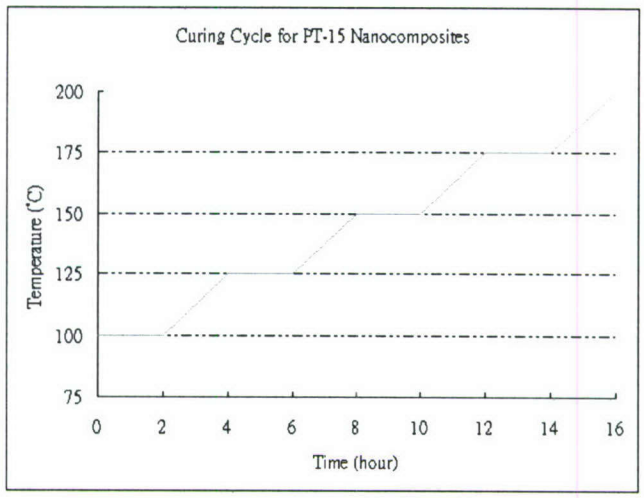

Figure 4-20 Curing cycle for all PT-15 nanocomposites.

Upon curing, no by-product gas is produced. A trace odor of PT-15 is noted, possibly from thermal decomposition of lower-molecular weight PT-15 within the polymer melt. Other than the occasional air bubble bursts within the 3wt% and 5wt% SDNT specimens, the curing cycle employed functions very well on the material. The finished and cured products are shown in Figure 4-21.

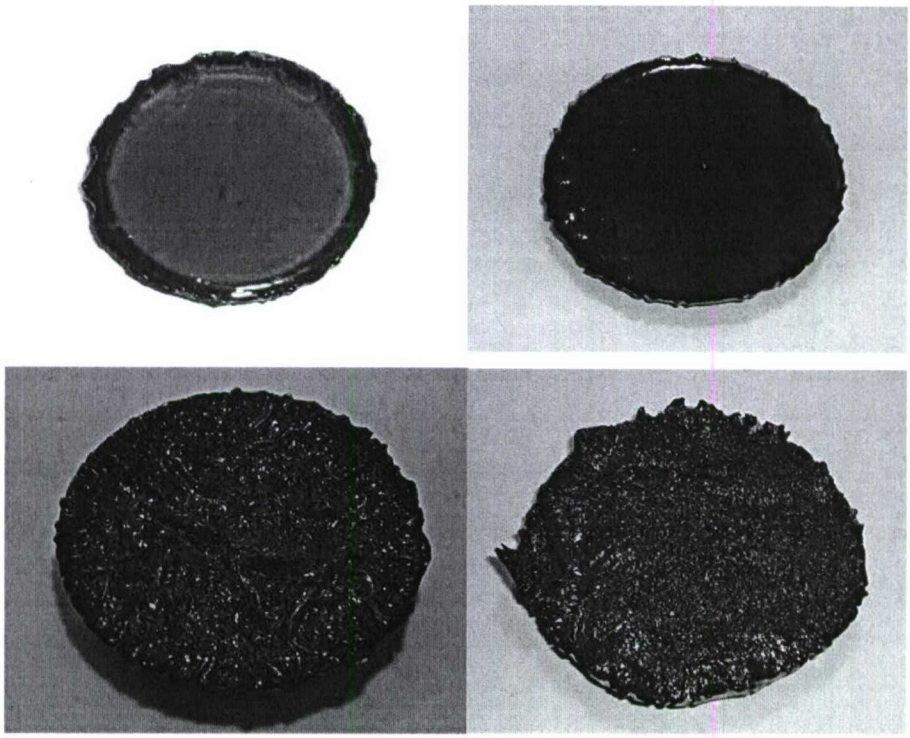

Figure 4-21 Cured PT-15 nanocomposites: neat PT-15 (upper left), 1wt%-buckytube/PT-15 (upper right), 3wt%-buckytube/PT-15 (lower left), 5wt%-buckytube/PT-15 (lower right). Specimen diameters are 6.35 cm (2.5 inches).

As expected, bubbles and gas evolution are apparent in the 3wt% and 5wt% specimens. Some voids are observable. This suggests that a better degassing procedure is needed. The surface finish for 3wt% and 5wt% SDNT is rugged and highly uneven as well. This suggests that the material viscosity remains high and would not flow even at curing temperature. This also suggests that the material is inherently non-processable.

It is important to note that phase separation is observed after curing. The cured product shows a clear black composite phase and a maple-orange PT-15 phase. This phenomenon is observed in all PT-15/SDNT nanocomposite specimens. Figure 4-22 depicts a thin-layer specimen of cured 1wt%-buckytube/PT-15. This type of phase separation is rarely seen in our nanocomposite studies. It indicates a severe incompatibility between the buckytubes and the PT-15 cyanate ester. This can be due to the fact that PT-15 is somewhat polar and nanotubes are non-polar. This is contrary to the earlier suggestion of CNI regarding untreated buckytubes dispersing well in polar resins. Functionalization of the buckytubes is proposed to create a more compatible interface with the PT-15 cyanate ester.

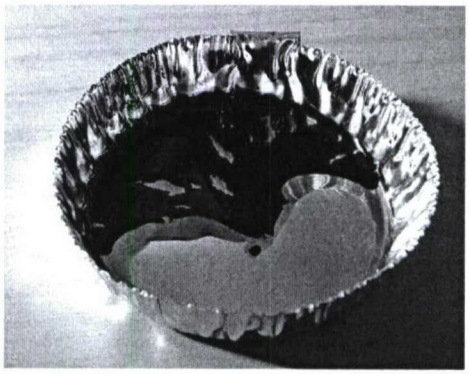

Figure 4-22 Phase separation: thin layer of cured 1wt%-buckytube/PT-15. The black region is the nanocomposite region and the orange is neat PT-15. Aluminum plate diameter is 6.35 cm (2.5 inches).

Selected SEM micrographs of buckytube/PT-15 nanocomposites are shown in Figure 4-23. It is observed that the buckytube forms clusters and bundles resulting in agglomerates. From the lower magnification micrographs, it can be easily seen that the buckytubes did not disperse and remain in clusters of a few microns in size. It is evident that the high shear from the colloid mixer is insufficient to disperse these buckytubes.

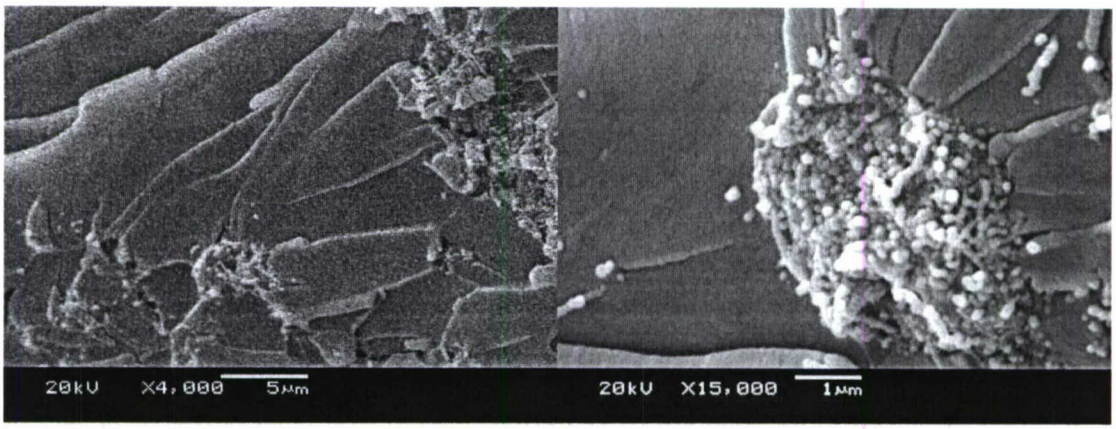

Figure 4-23 4kX (left) and 15kX (right) SEM micrographs of 1wt%-buckytube/PT-15 nanocomposite.

Figures 4-24 to 4-26 show TEM micrographs of buckytube/PT-15 nanocomposites. A mediocre dispersion for the 1wt%-buckytube/PT-15 nanocomposite is observed. The typical cluster size is about 1 micron. Figure 4-25 shows a similar cluster size for the 3wt%-buckytube/PT-15 formulation. Though in some isolated cases there are a few dispersed buckytubes, agglomeration is by far most prominent. It is thus logical to conclude that the existing processing parameters would yield micron-size aggregate clusters and would not disperse.

For the 5wt%-buckytube/PT-15 formulation, agglomeration is dominant and the cluster size is nearly several microns. The apparent failure for the 5wt%-buckytube system is likely due to processing limitations. As previously discussed, the high viscosity inhibits a thorough shear mixing for the system.

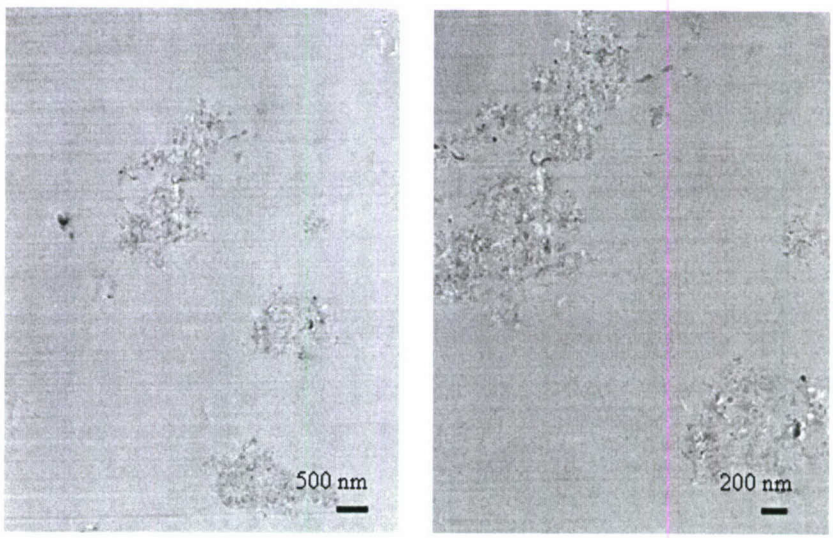

Figure 4-24 TEM micrographs of 1wt%-buckytube/PT-15 nanocomposite, 10kX half micron scale bar on the left, and 20kX 200nm scale bar on the right.

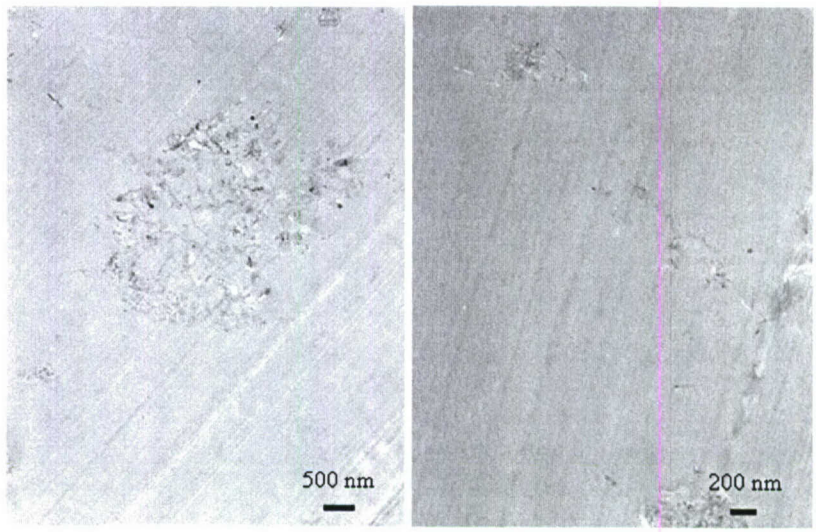

Figure 4-25 TEM micrographs of 3wt%-buckytube/PT-15 nanocomposite, 10kX half micron scale bar on the left, and 20kX 200nm scale bar on the right.

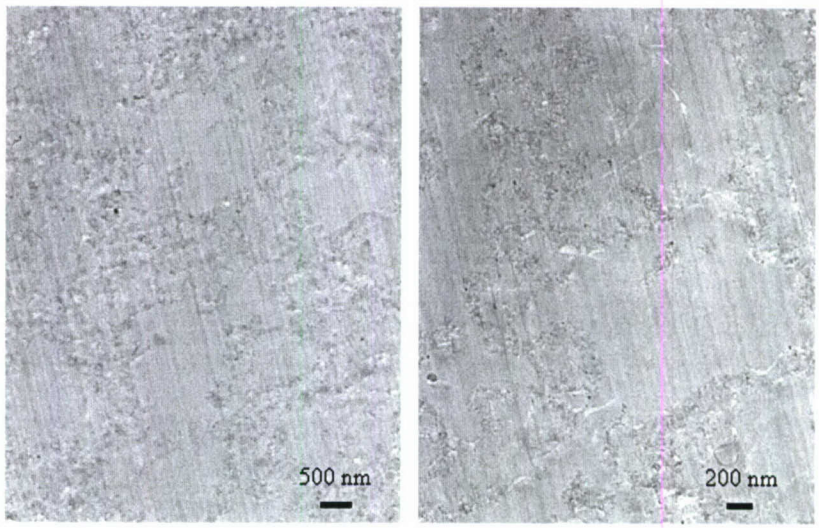

Figure 4-26 TEM micrographs of 5wt%-buckytube/PT-15 nanocomposite, 10kX half micron scale bar on the left, and 20kX 200nm scale bar on the right.

Overall, TEM observations are consistent with SEM results. It shows clustering and agglomerations, and proves that the high shear process by IKA colloid mixer fails to disperse buckytubes into PT-15.

Thermal Stability of PT-15/Buckytubes Systems - TGA was performed on all specimens under air at three different heating rates: 5°C/min, 10°C/min, and 20°C/min. The results of the three nanocomposite products are compared to the neat PT-15 system. They are shown in Figures 4-27 to 4-29.

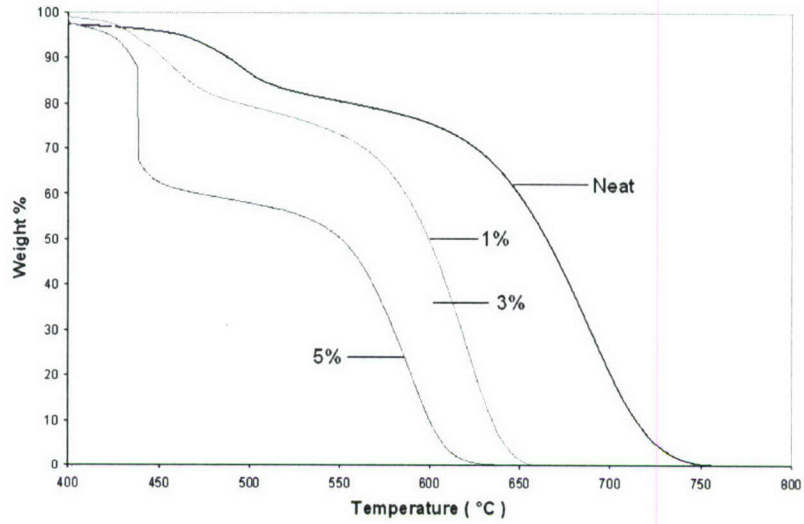

Figure 4-27 TGA for PT-15/buckytube nanocomposites, 5°C/min.

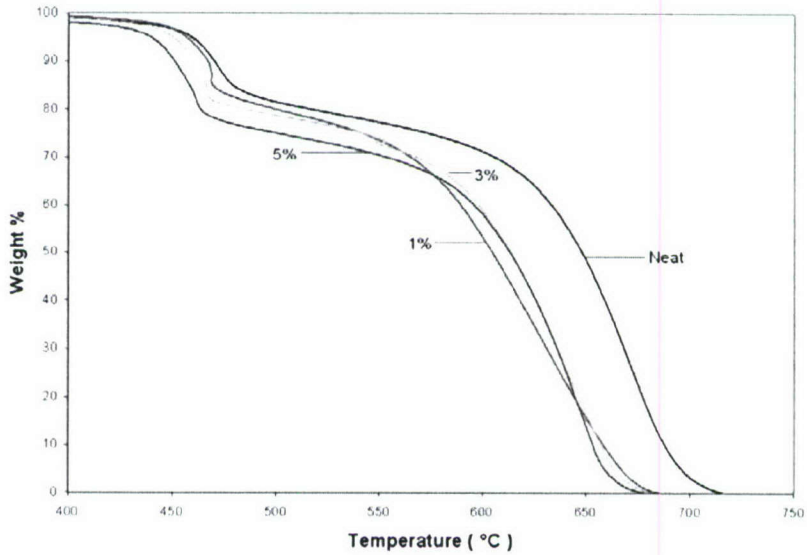

Figure 4-28 TGA for PT-15/buckytube nanocomposites, 10°C/min.

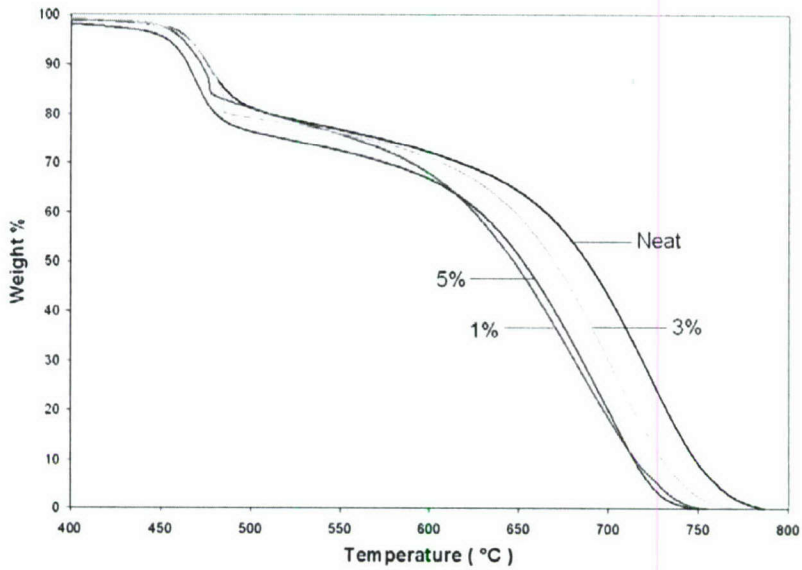

Figure 4-29 TGA for PT-15/buckytube nanocomposites, 20°C/min.

It can be noted that decomposition for the neat PT-15 system begins at around 450°C, and is consistent with the value provided by Lonza Corp. In all instances, the introduction of buckytube lowers the thermal stability of the PT-15 system. At lower heat rates, this adverse effect is more pronounced; and it is apparent that the more buckytube added, the worse the system behaves thermally. For 5wt% buckytube, decomposition temperature is lowered by 50°C. For the others, a 20-30°C decrease is observed.

The decrease in decomposition temperature is likely a result of the thermal conductive nature of the buckytube. Although there is an observable phase separation and a high possibility of poor dispersion, the decomposition temperature is not expected to decrease (from other PT-15 nanocomposite studies). In the worst case of agglomeration, the decomposition temperature would simply remain unchanged. A decomposition temperature depression is thus more likely a result from increased heat conduction rather than decreased thermal stability from chemical change. However, further investigation is needed to verify this hypothesis.

Glass Transition Temperature - Similar to TGA, DSC is performed on all PT-15-buckytube specimens and compared to the neat PT-15 system. The characterization temperature range is 50°C to 400°C under air, and at three different heating rates: 5°C/min, 10°C/min, and 20°C/min. The results are shown in Figures 4-30 to 4-32.

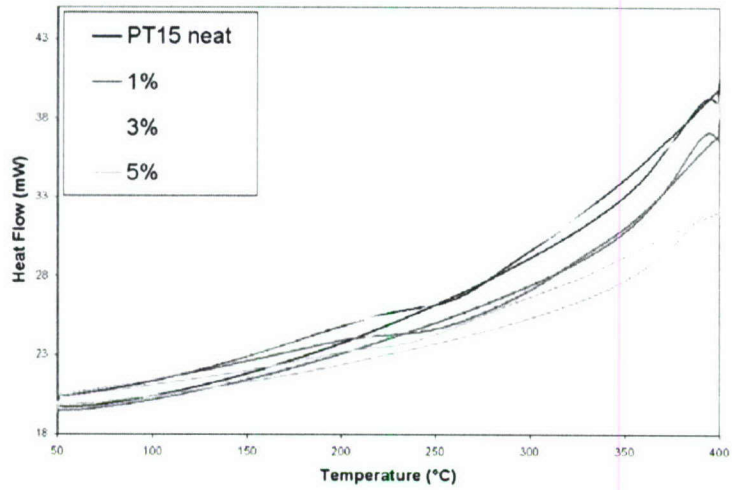

Figure 4-30 DSC for PT-15/buckytube nanocomposites, 5°C/min.

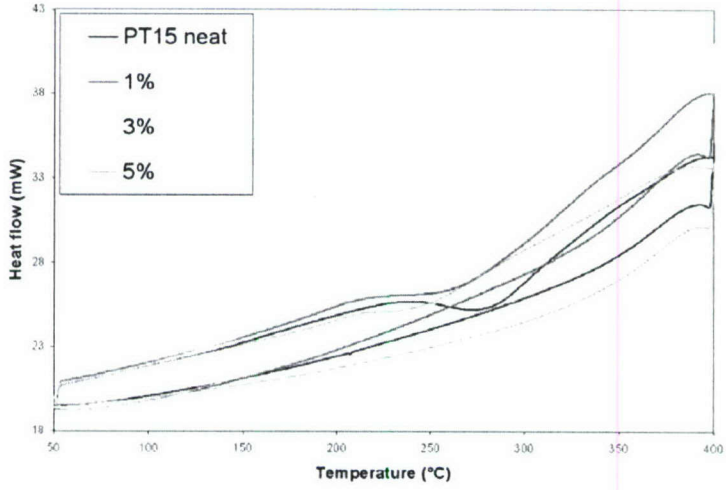

Figure 4-31 DSC for PT-15/buckytube nanocomposites, 10°C/min.

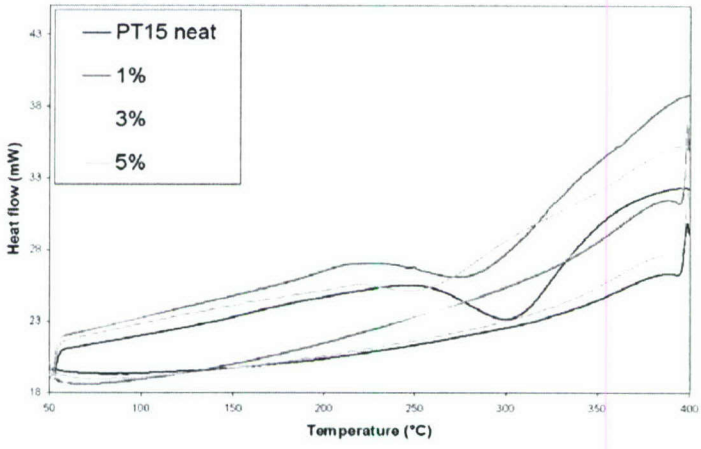

Figure 4-32 DSC for PT-15/buckytube nanocomposites, 20°C/min.

The peak at around 300°C to 350°C is the melting peak. It is apparent that a melting point depression is prominent in all specimens (relative to neat PT-15), by 20-50°C. This can be caused by impurity effects, wherein the buckytube phase acts as an impurity and induces an entropic effect. This can also be a result of the thermal conduction previously mentioned. The observations made in DSC are consistent with those obtained in TGA, and that the thermal profile of PT-15 is shifted to a lower temperature by 15-50°C with the introduction of buckytubes.

The glass transition temperature (T_g) is obtained by extrapolating to the temperature at which there is a change in slope of the thermal profile. A discontinuity in the slope of the profile gives the temperature at which the material undergoes a second order kinetic transition, which is what the glass transition temperature is. Table 4-3 shows the measured glass transition temperatures of various PT-15/ buckytube nanocomposites.

Table 4-3 Glass Transition Temperatures for PT-15/ buckytube Nanocomposites

Heating Rate	Neat PT-15	1wt% buckytube	3wt% buckytube	5wt% buckytube
5°C/min	351°C	348°C	342°C	335°C
10°C/min	353°C	341°C	331°C	298°C
20°C/min	363°C	353°C	353°C	311°C

It is apparent that the introduction of buckytube does not increase the T_g at all. In the case with 5wt% buckytube, a substantial decrease in T_g is measured. For the other formulations, there is a slight to moderate decrease in T_g as well. This is in agreement with the decrease in T_g and decomposition temperature measured.

Because of the imprecise nature of the extrapolation process, some uncertainty is expected. Also, under different heating rates, different glass transition temperatures are measured. This is due to the variable polymer material response time under different thermal conditions. For a more accurate assessment of glass transition temperature, dynamic mechanical thermal analysis (DMTA) is typically used. Yet, due to the failure to degas the viscous PT-15/buckytube nanocomposites, DMTA samples cannot be made. Thus, to fully address this issue, solution conditions may be required to resolve the viscosity problem.

Summary and Conclusions

- High polymer viscosity of PT-15/buckytube systems results in a severe processing limitation on the IKA mixer; and over time, as nanoparticles disperse, the melt viscosity drastically increases and obstructs the processing flow.
- For CE-buckytube nanocomposite synthesis, 3wt% of buckytube is the maximum processible limit because of the viscous obstruction. It is also found that premixing and preheating the mixture facilitates the initial startup of the process.
- Similar thermal curing cycles are used for all formulations of CE-buckytube nanocomposites.
- The IKA colloid mixer suspends a large volume of entrapped air in the PT-15/buckytube system.
- For CE-1wt%buckytube, degassing is successful by vacuum heating. For the others, the

viscosity remains tar-like up to the curing temperature, and thus air is trapped in the polymer and voids are observed in the specimen.

- For all specimens, a phase separation is observed: an orange neat phase (PT-15) is separated from a black composite phase.
- From SEM and TEM micrographs, the IKA high shear colloid mixer is not able to disperse buckytube into the PT-15 cyanate ester resin when the concentration of buckytubes is 3% or greater.
- Buckytube clusters and agglomerates of a few microns in size are observed for high amounts (3%) of buckytubes in PT-15. These are proposed as evidence of inherent material incompatibility.
- Functionalization of the buckytube is recommended to enhance dispersion.
- In previous studies, it has been shown that the IKA colloid mixer performs very well for aqueous systems with nanoclay with no attendant viscosity issues, while the processing of viscous polymers is possible but difficult.
- Buckytube fails to disperse in PT-15 CE because of processing limitations and fundamental material incompatibility.

4.6 Fabrication and Characterization of Carbon/Carbon Composites [47-49]

PT-15 CE Resin/Nanoparticle Systems - Four PT-15/nanoclay and PT-15/POSS nanocomposites with T-300 3K carbon fabric were fabricated into CCCs using the CVI process. All of the CCC panels being fabricated are approximately 12- by 12- by 0.15-inches (Group A).

AR Mesophase Pitch Monomer - Three different groups of CCC panels were fabricated with AR mesophase pitch monomer and T300 3K fabric using the SMJ Carbon in-situ polymerization method. All of the C-C panels being fabricated are approximately 6- by 6- by 0.125-inches.

The first group of panels involved the use of 50 nm SiC nanoparticles as an additive to the AR carbon matrix (Group B). Five different SiC loading levels were used. They are 0, 5, 10, 15, and 20% by weight. The SiC particles were thoroughly mixed with AR mesophase powder and hot pressed. The panels were pressed at ~ 375°C under ~ 450 psi. Each panel was subsequently oxidative stabilized at 220°C for 100 hours. These panels were carbonized to 1000°C before being densified. The target density for these panels is ~1.7 g/cc. After 3 impregnation cycles, the weight gain was unchanged. To reopen the porosity in the composites, they were heat treated to 1700°C and facilitated their completion.

The second group of composite panels was fabricated identically to those described above (Group C). Once densified to ~ 1.5 g/cc with a carbon matrix, these parts were vacuum impregnated with Ceraset™ resin and heat treated to 1000°C. These parts were impregnated with Ceraset™ until weight gain ceased. This group was completed.

The final group of composites is being fabricated in a very similar fashion with one major difference (Group D). The fabric plies are being coated with a very thin layer of preceramic polymer and heat treated to 1000°C to convert this polymer to amorphous SiC. These plies are then hot pressed with SiC loaded AR resin and fabricated in a similar fashion as above. Five candidates will be fabricated for this group and the fabrication is in progress.

Fabrication - In summary, based on TEM, TGA, and DSC analyses, and scale up studies, fourteen (14) candidates divided into three groups (Groups A to C) were fabricated into CCC panels using T-300 3K fabric and two processing methods listed as follows:

Group A – CVI Process

- PT-15 CE in 100 wt% (baseline C-C composite)
- PT-15 CE/Cloisite® 30B in (95/5) wt%
- PT-15 CE/SO1458 POSS® in (95/5) wt%
- PT-15 CE/imidazolium-treated nanoclay (95/5) wt%

Group B – In-Situ Polymerization Process

- AR mesophase pitch in 100 wt%
- AR mesophase pitch/n-SiC in (95/5) wt%
- AR mesophase pitch/n-SiC in (90/10) wt%
- AR mesophase pitch/n-SiC in (85/15) wt%
- AR mesophase pitch/n-SiC in (80/20) wt%

Group C - In-Situ Polymerization Process

- AR mesophase pitch in 100 wt% impregnated with Ceraset™
- AR mesophase pitch/n-SiC in (95/5) wt% impregnated with Ceraset™
- AR mesophase pitch/n-SiC in (90/10) wt% impregnated with Ceraset™
- AR mesophase pitch/n-SiC in (85/15) wt% impregnated with Ceraset™
- AR mesophase pitch/n-SiC in (80/20) wt% impregnated with Ceraset™

Group D - In-Situ Polymerization Process – In Progress

- AR mesophase pitch in 100 wt% with fabric coating
- AR mesophase pitch in 100 wt% impregnated with Ceraset™ with fabric coating
- AR mesophase pitch/n-SiC in (90/10) wt% impregnated with Ceraset™ with fabric coating
- AR mesophase pitch/n-SiC in (85/15) wt% impregnated with Ceraset™ with fabric coating
- AR mesophase pitch/n-SiC in (80/20) wt% impregnated with Ceraset™ with fabric coating

Group E - Fabricated by DACC

- C/C composite with 3D carbon fiber perform (with no anti-oxidation coating) was fabricated by CVD densification with final 220°C heat treatment
- C/SiC composite with 2D 12K carbon fiber perform (with no anti-oxidation coating) was fabricated by SMI (DACC proprietary) process (1650°C siliconizing)

Density and Microstructural Analyses of Pre-test Specimens - Figure 4-33 shows the density of two sets of CCC, one is fabricated using AR mesophase pitch (MPP) incorporated with n-SiC and the other is using AR mesophase pitch and SiC infused with Ceraset™ preceramic resin. For the set of CC-SiC MPP, the baseline has the lowest density, which is 1.41g/cc, while the one with 10 wt% loading of n-SiC has the highest density, which is 1.76g/cc. This can be explained by the subsequent microstructural analyses discussion.

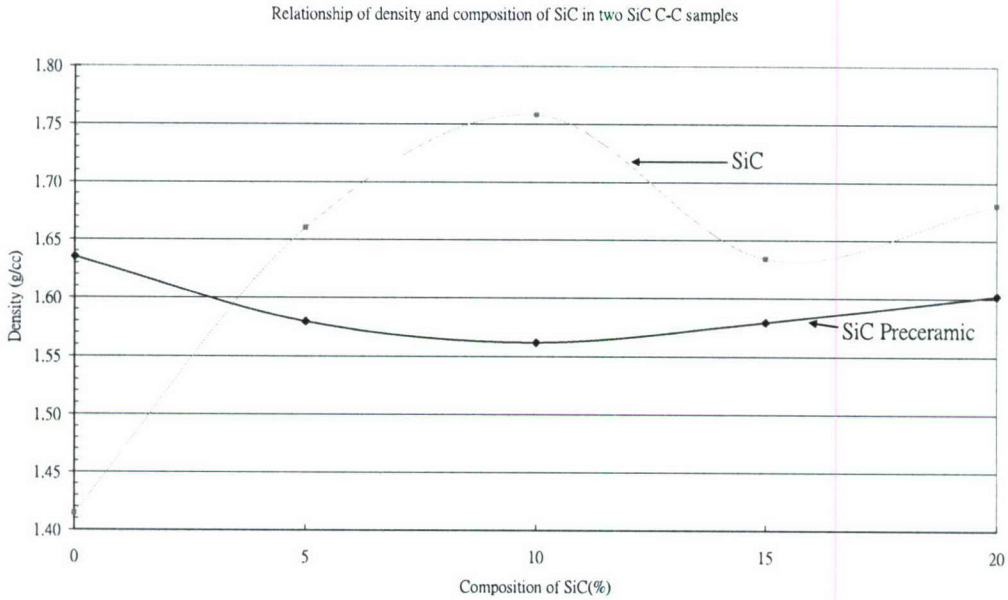

Figure 4-33 Density of C-C samples with 0%, 5%, 10%, 15%, and 20% n-SiC.

Figure 4-34 shows the SEM micrographs of five different weight loadings of CC-SiC MPP. Among the five CC-SiC MPP samples, it was observed that the baseline has the largest number of micro-voids, while the 10% one has the least. The number of voids in ascending order is the 5%, 15% and 20% samples, less than that in the baseline but more than that in the 10% sample. Therefore, it can be related that the sample, which has a higher density has less number of voids.

For the set of CC-SiC preceramic, the baseline has the highest density (1.64g/cc), while the 10% CCC sample has the lowest density (1.56g/cc). Figure 4-35 shows the SEM micrographs of the five different weight loadings of CC-SiC preceramic. They also follow the observation that the higher their densities, the less number of voids they have. The largest void observed is over 600μm in length and over 100μm in width.

Since the n-SiC used in the two sets of CCC is the same, the difference in density change in the two sets might be due to the compatibility between the n-SiC and the matrices used in the CCC. The n-SiC seems to have a better compatibility with the mesophase pitch than with the preceramic.

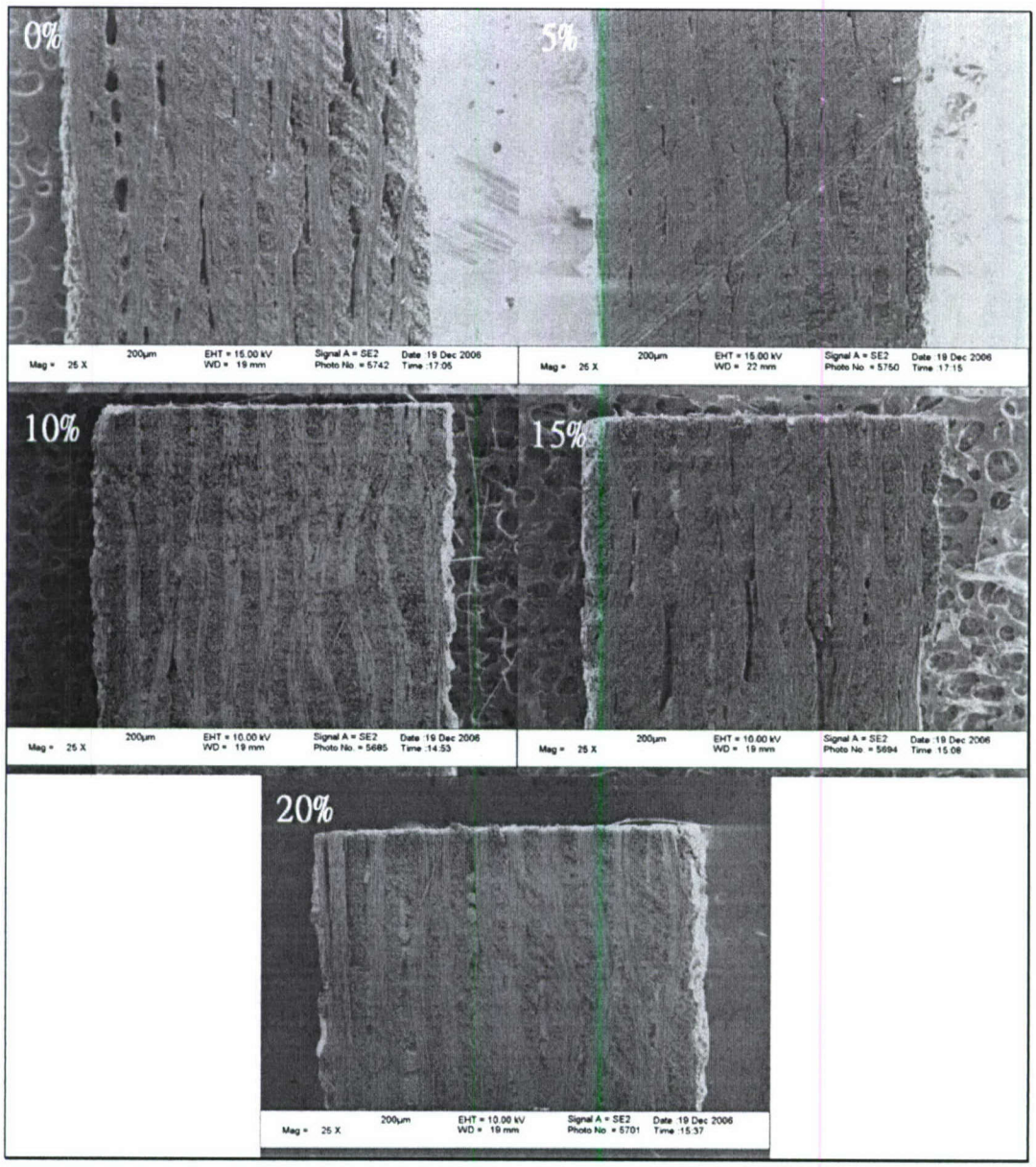

Figure 4-34 SEM micrographs of CCC mesophase pitch samples with 0%, 5%, 10%, 15%, and 20% n-SiC, respectively.

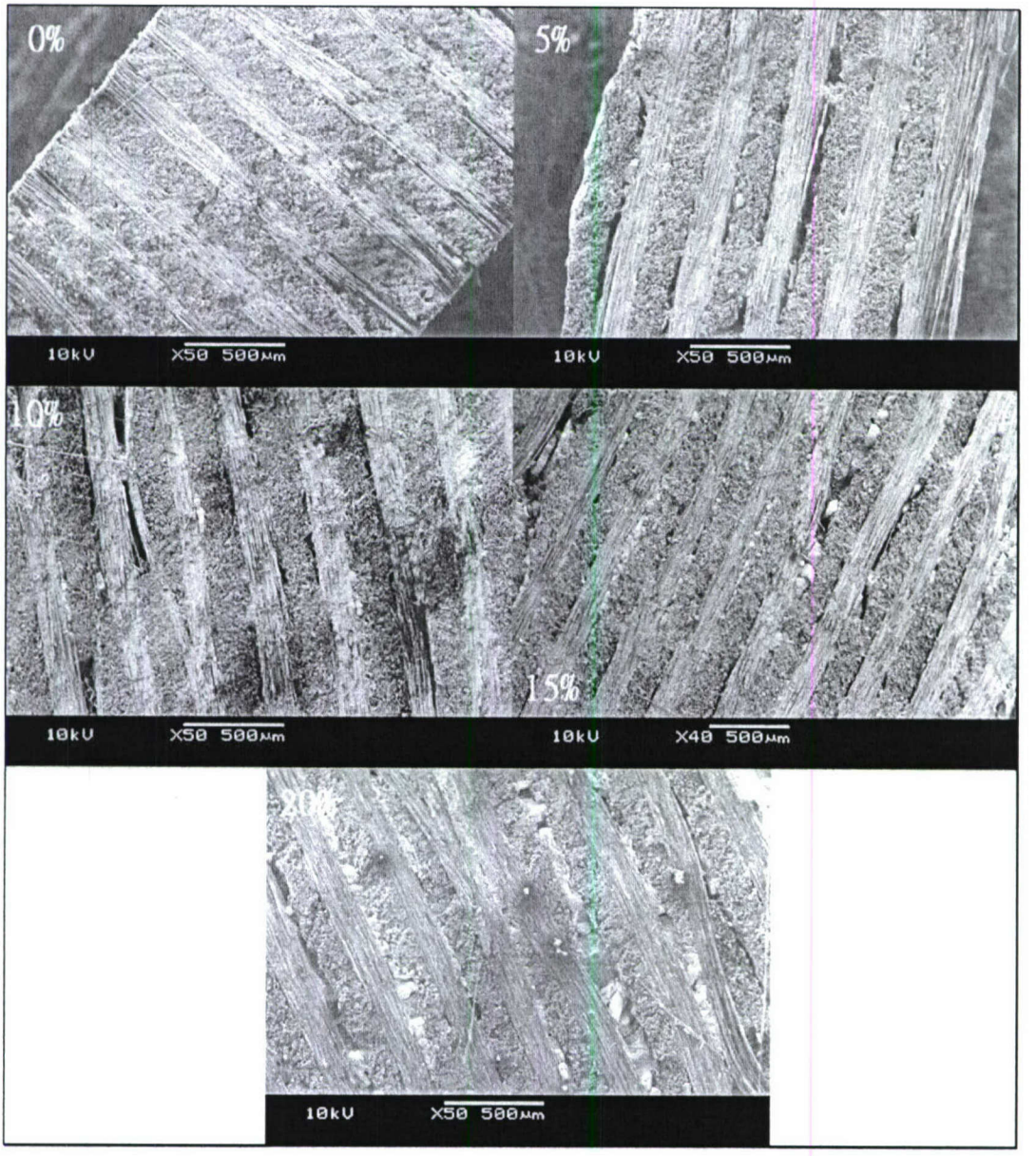

Figure 4-35 SEM micrographs of CCC preceramic samples with 0%, 5%, 10%, 15%, and 20% n-SiC, respectively.

Figure 4-36 shows the density of three CCCs, namely KAI baseline (PT-15 resin only), KAI-CB (PT-15 with 5 wt% Cloisite 30B), and KAI-POSS (PT-15 with 5 wt% Trisilanlophenyl-POSS). The KAI-CB has slightly higher density than the other two. The difference in density for this set of CCC is less than 3%. According to the SEM micrographs as shown in Figure 4-37, the number of voids in all three samples is about the same. This explains why their densities do not deviate much.

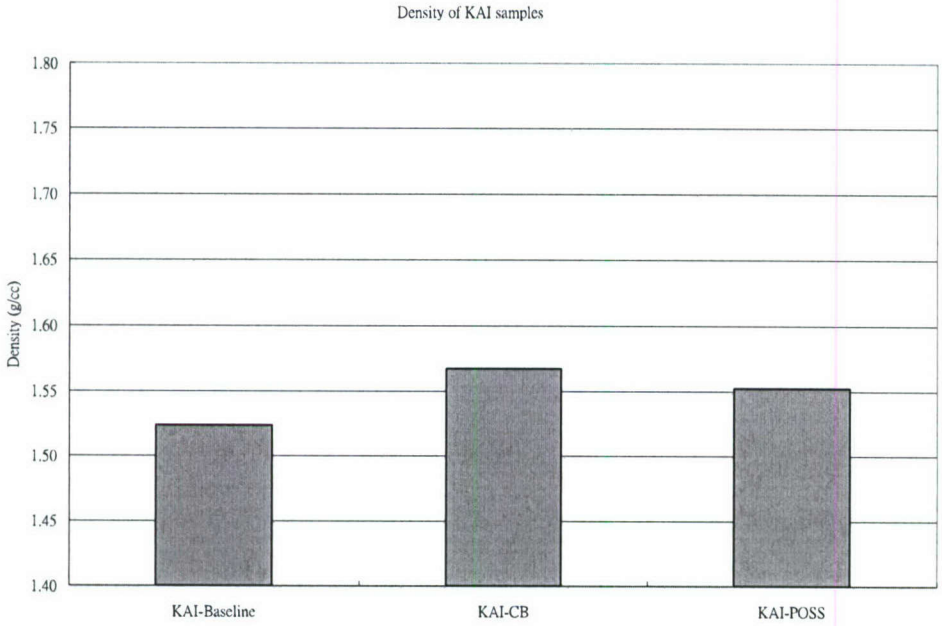

Figure 4-36 Density of KAI C-C samples: KAI baseline (PT-15), KAI-CB (PT-15 with nanoclay), and KAI-POSS (PT-15 with POSS).

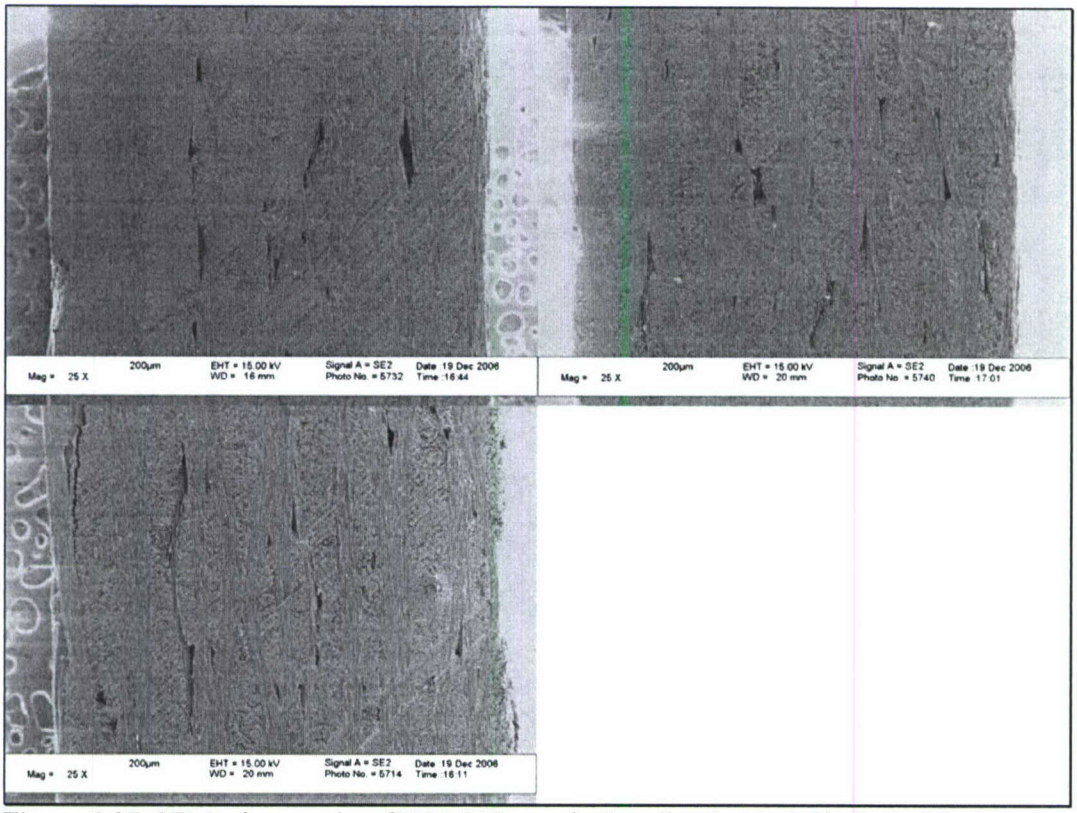

Figure 4-37 SEM micrographs of KAI C-C samples baseline (upper left), C-C with clay (upper right), and C-C with POSS (lower left).

Additional microstructural analyses of the NCCC samples were conducted using optical microscopy with x50 and x100 magnifications. We observed the CE based CCC (PT-15, PT-15/5wt% 30B, PT-15/5wt% POSS, and PT-15/5 wt% Imidazolium-treated nanoclay samples) have relatively uniform microstructures with some voids while the AR mesophase pitch based CCC (SiC and SiC with preceramic) have non-uniform structures and voids. The mesophase pitch based CCC have more dense microstructures at the side than the center area. Figure 4-38 shows optical micrographs at x50 magnification of the PT-15/5%Closite 30B NCCC (a) center view and (b) side view; and AR 0%SiC with preceramic NCCC (c) center view and (d) side view; and AR 10%SiC with preceramic NCCC (e) center view and (f) side view.

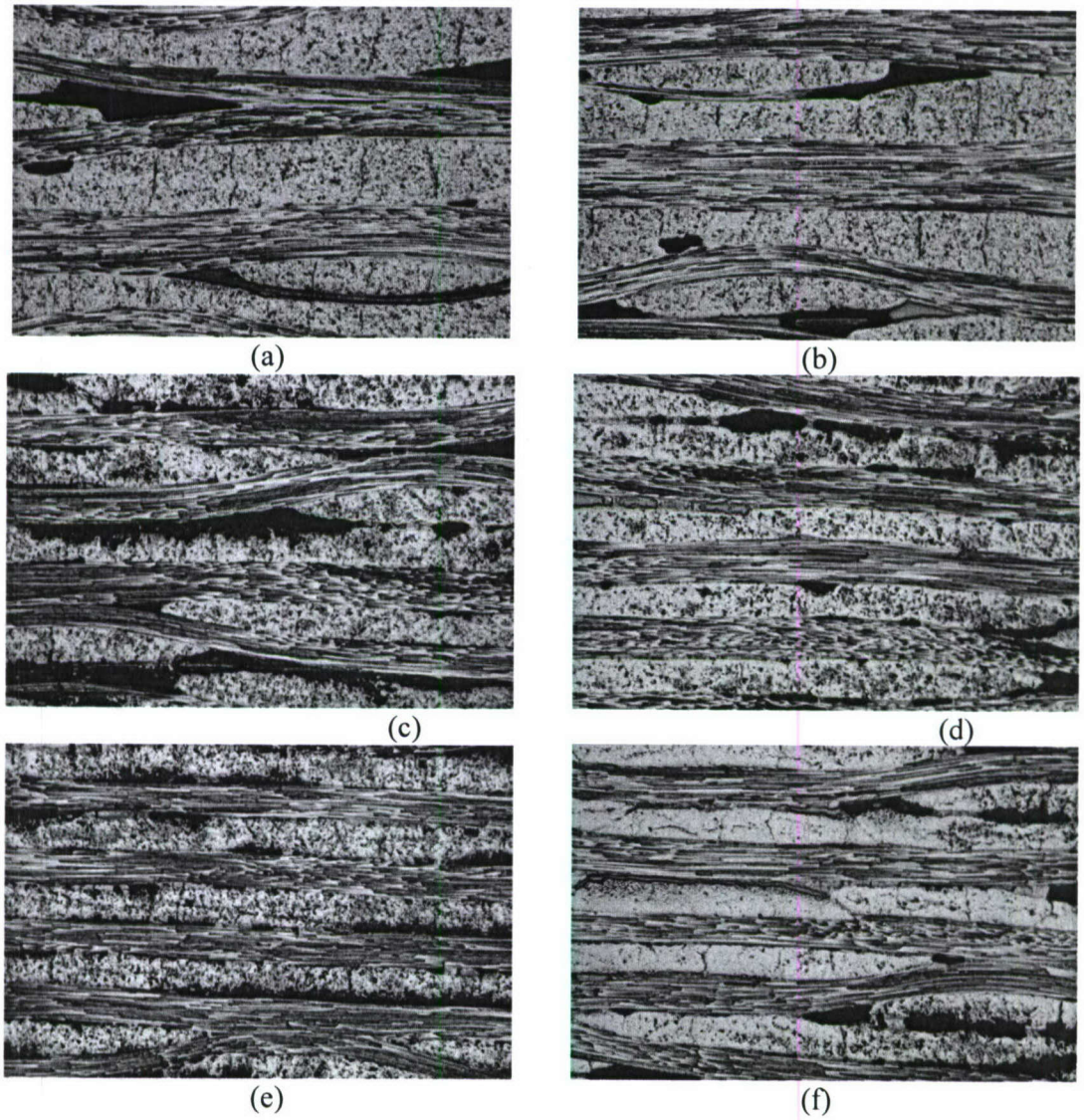

Figure 4-38 Optical micrographs at x50 magnification of PT-15/5%Closite 30B NCCC (a) center view and (b) side view; AR 0%SiC with preceramic NCCC (c) center view and (d) side view; AR 10%SiC with preceramic NCCC (e) center view and (f) side view.

Thermo-oxidative Studies of NCCC Samples - Two types of heat-aged tests were used to determine the thermo-oxidative resistant of the four groups of CCCs. All NCCCs were heated at 650°C for 100 hrs using a vacuum furnace. All materials were also heated to 900°C using TGA in air. Airflow rate of 200 cc/min at heating rate of 20°C/min were used for the TGA experiments. Table 4-4 shows a summary of the density, mass loss for the vacuum furnace and TGA under air experiments for the four groups of CCCs. TGA rankings of the panels are shown at the right of the table and are discussed fully when considering subsequent figures.

Table 4-4 Summary of Density, Mass Loss, and TGA data of Four Groups of NCCCs and C/SiC

Candidates	Group	Density (g/cc)	Mass Loss (%)[1]	TGA[2]	TGA[3]
KAI-Baseline (PT-15 resin only)	A	1.52	0		
KAI-CB (PT-15/Cloisite 30B :95/5 wt%)	A	1.57	-0.58%		
KAI-POSS (PT-15/SO1454 POSS:95/5 wt%)	A	1.55	0		
KAI-IM (PT-15/imidazolium-treated nanoclay: 95/5 wt%)	A	1.64	Not tested	3	4
AR mesophase pitch in 100 wt%	B	1.41	0.73		3
AR mesophase pitch/n-SiC in (95/5) wt%	B	1.66	3.5		
AR mesophase pitch/n-SiC in (90/10) wt%	B	1.76	0.84	4	
AR mesophase pitch/n-SiC in (85/15) wt%	B	1.63	1.04		
AR mesophase pitch/n-SiC in (80/20) wt%	B	1.68	0.96		
AR mesophase pitch in 100 wt% impregnated with Ceraset™	C	1.64	0.0	2	2
AR mesophase pitch/n-SiC in (95/5) wt% impregnated with Ceraset™	C	1.58	0.03		
AR mesophase pitch/n-SiC in (90/10) wt% impregnated with Ceraset™	C	1.56	0.0		
AR mesophase pitch/n-SiC in (85/15) wt% impregnated with Ceraset™	C	1.58	0.0		
AR mesophase pitch/n-SiC in (80/20) wt% impregnated with Ceraset™	C	1.60	0.0		
DACC C/C Composite	E	1.75	NA		
DACC C/SiC Composite	E	2.1	NA	1	1

[1]Heat-aging for 50 hrs at 650°C in vacuum.
[2]TGA dynamic experiments were conducted with airflow of 200 cc/min at a heating rate of 20°C/min.
[3]TGA heat-soaking experiments (650°C for 5 hrs.) were conducted with airflow of 200 cc/min at a heating rate of 20°C/min.

TGA Analysis - Two types of TGA analyses were conducted: (a) Materials were exposed from room temperature (RT) to 900°C (dynamic measurement) with heating rate of 20°C/min and air

purging rate at 200 cc/min and (b) Materials were soaking at 650°C with heat rating of 20°C/min and air purging rate at 200 cc/min for 5 hrs. Figures 4-39 to 4-43 show the 900°C dynamic TGA measurements for Groups A to E and the best candidate from each group (Figure 4-43).

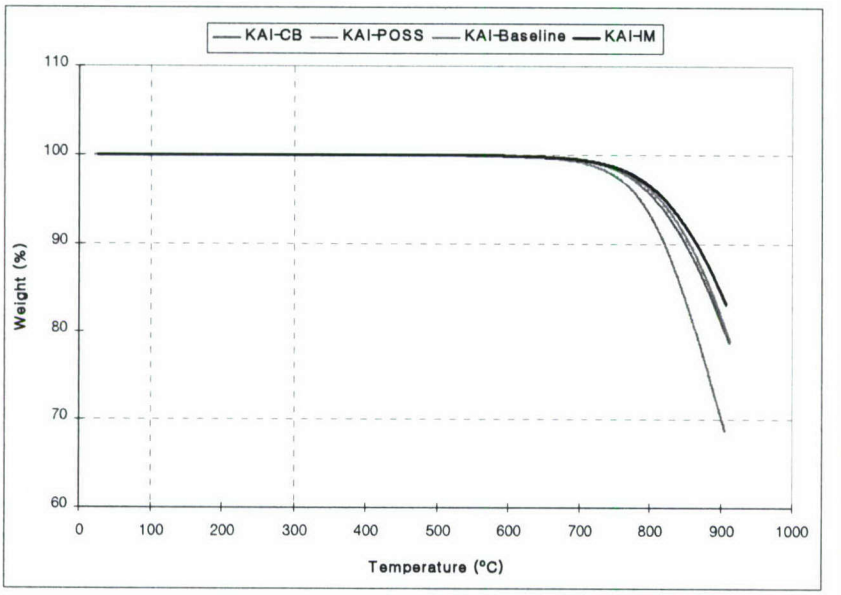

Figure 4-39 TGA dynamic measurements of Group A: KAI-CB, KAI-POSS, KAI-Baseline, and KAI-IM composites.

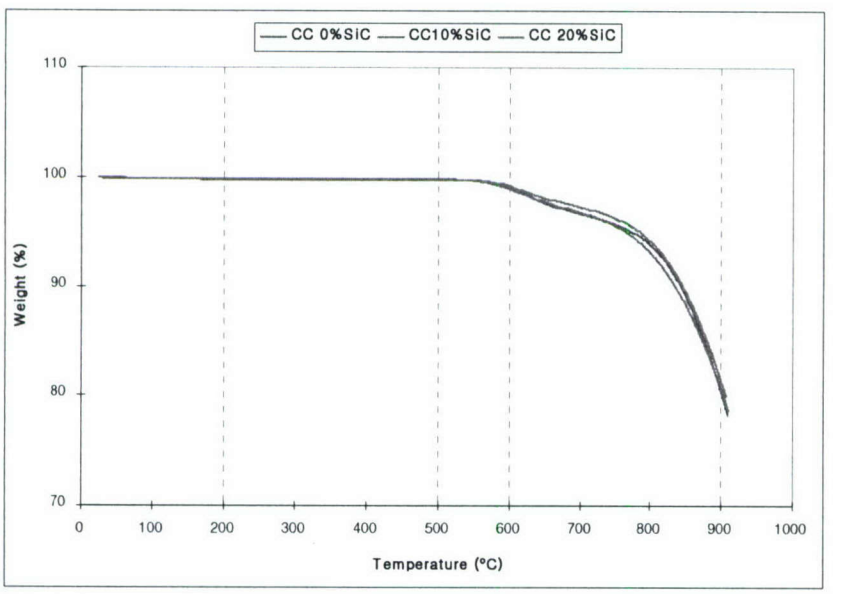

Figure 4-40 TGA dynamic measurements of Group B: CC 0% SiC, CC 10% SiC, and CC 20% SiC composites.

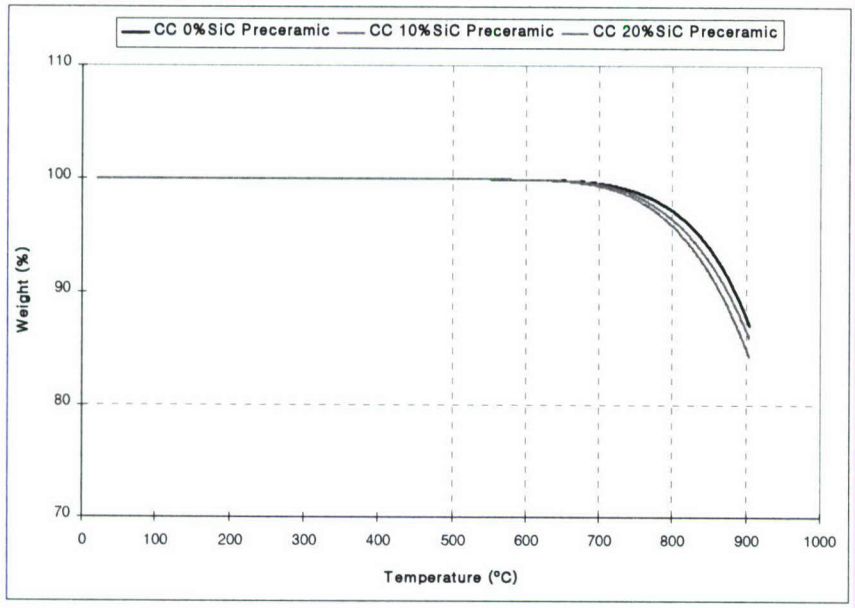

Figure 4-41 TGA dynamic measurements of Group C: CC 0% SiC Precreamic, CC 10% SiC Preceramic, and CC 20% SiC Preceramic composites.

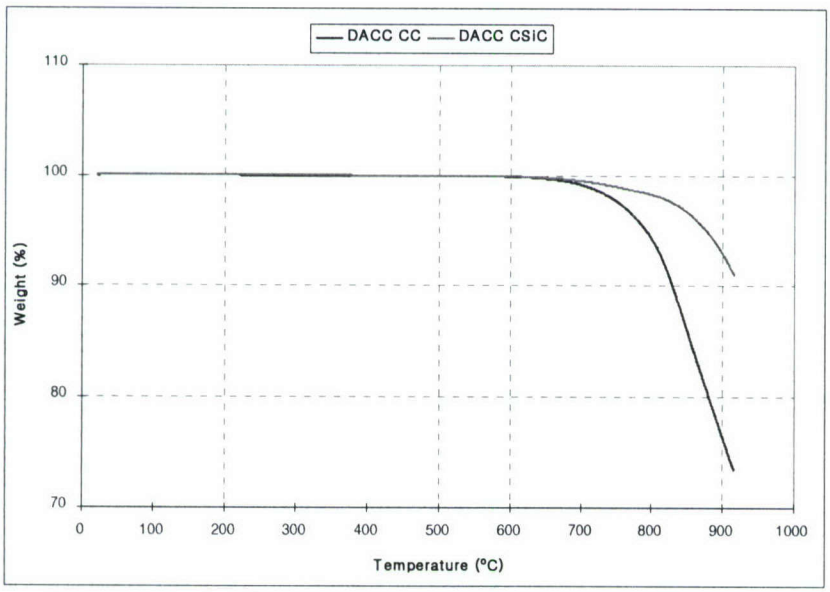

Figure 4-42 TGA dynamic measurements of Group E: DACC C/C and DACC C/SiC composites.

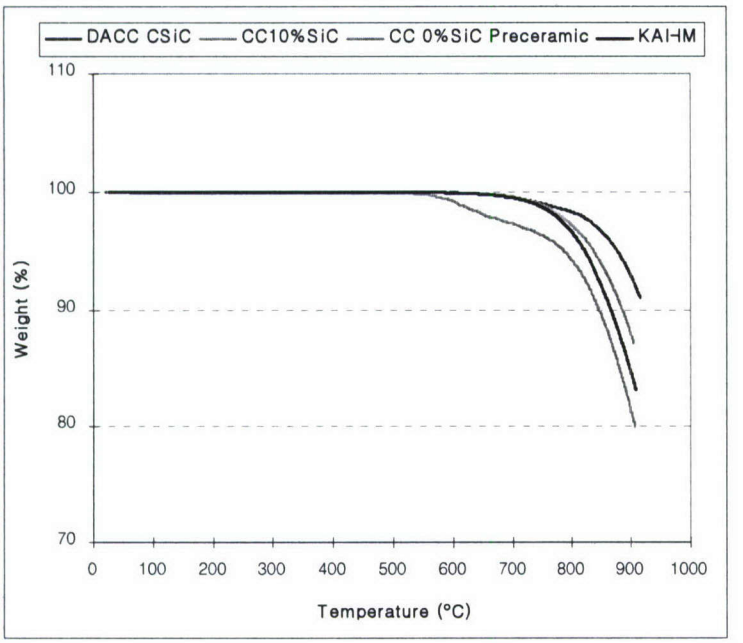

Figure 4-43 TGA dynamic measurements of the best materials of Groups A to C, and E.

Figures 4-44 to 4-48 show the 650°C soaking experiments for Groups A to C, and E and the best candidate from each group (Figure 4-48).

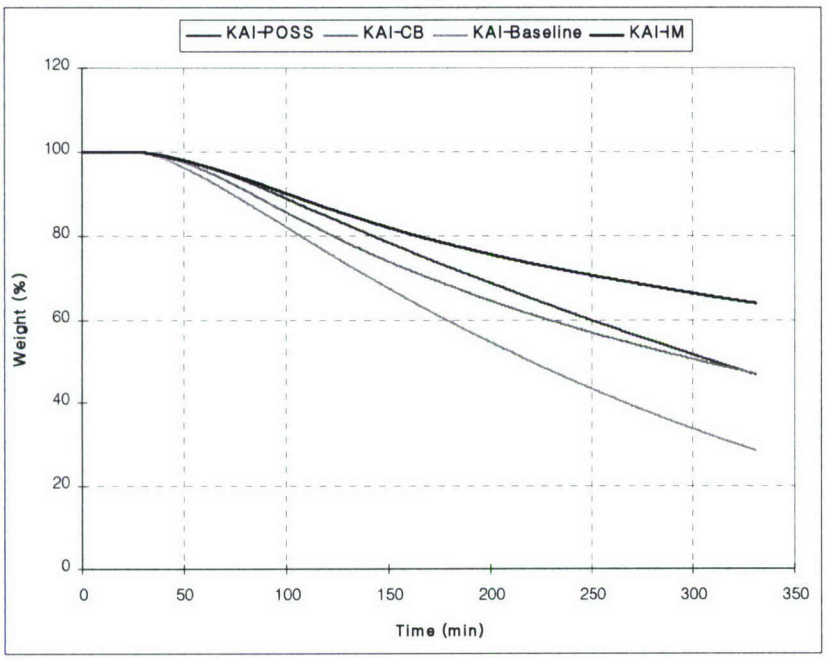

Figure 4-44 TGA 650°C soaking measurements of Group A: KAI-CB, KAI-POSS, KAI-Baseline, and KAI-IM composites.

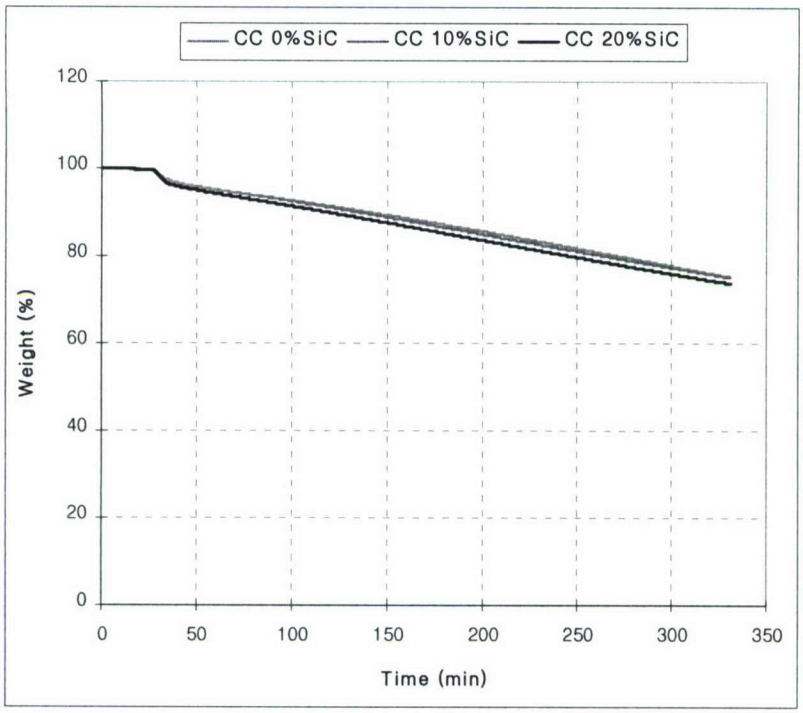

Figure 4-45 TGA 650°C soaking measurements of Group B: CC 0% SiC, CC 10% SiC, and CC 20% SiC composites.

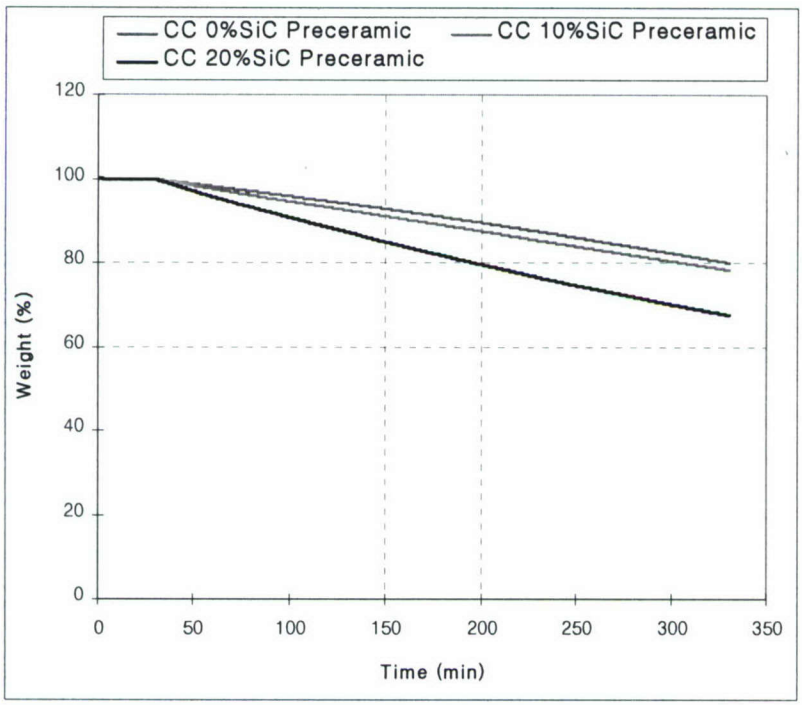

Figure 4-46 TGA 650°C soaking measurements of Group C: CC 0% SiC Precreamic, CC 10% SiC Preceramic, and CC 20% SiC Preceramic composites.

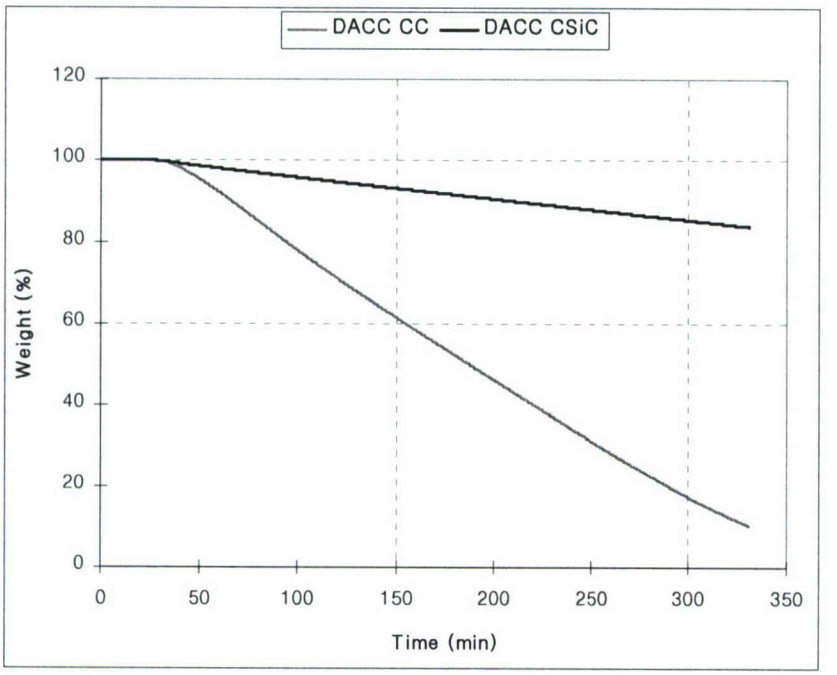

Figure 4-47 TGA 650°C soaking measurements of Group E: DACC C/C and DACC C/SiC composites.

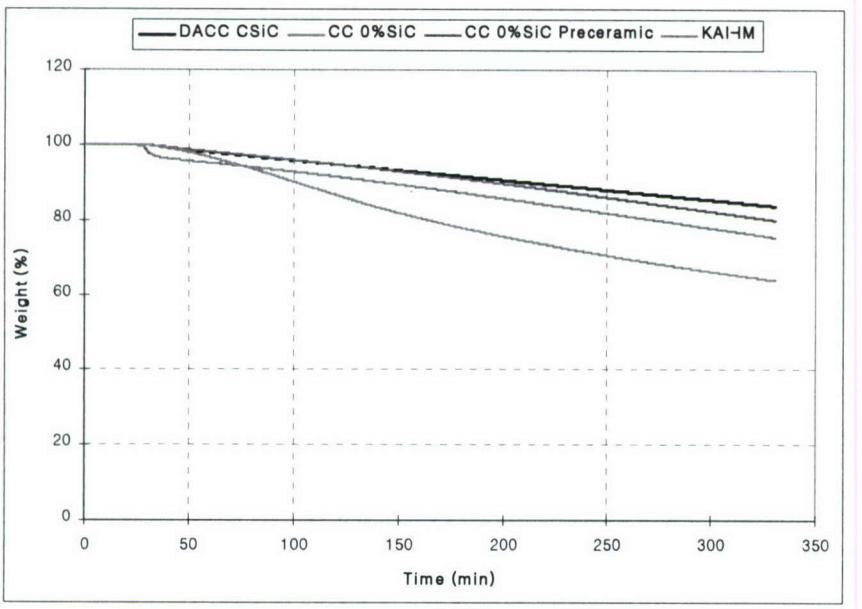

Figure 4-48 TGA 650°C soaking measurements of the best materials of Groups A to C and E.

It is clear from Figure 4-48, KAI-IM is the best candidate from Group A, CC 0% SiC is the best candidate from Group B, CC 0% SiC Preceramic is the best candidate from Group C, and DACC C/SiC is the best candidate from Group E. When the best candidate from each group was compared with each, the DACC C/SiC material is the most thermo-oxidative resistant, followed by the CC 0% SiC Preceramic, then the CC 0% SiC material, and the worst candidate is KAI-IM material.

Vacuum Furnace Heat Aging Test - Heat aging at 650°C for long duration (50 hrs) thermo-oxidative experiment supported the same observation. SiC samples [Group B] undergo mass loss of 1 to 3% when they were heated at 650°C for 50 hours under vacuum. Neither PT-15 [Group A] nor SiCp [Group C] had more than 0.5% mass loss when they were under the same experimental condition. DACC composites [Group E] were not tested using the vacuum furnace.

Both PT-15 and SiCp had a little mass loss when the temperature was less than 750°C. The PT-15 baseline began to lose mass severely when the temperature was at 800°C. The other PT-15 samples (PT-15 with nanoclay and POSS nanocomposites) performed similar to SiCp when the temperature was at 800°C. However, when the temperature reached 850°C, all PT-15 CCC samples started to lose mass more rapidly than SiCp CCC. This trend became obvious when all PT-15 CCC had higher mass loss than SiCp CCC samples eventually at 900°C.

The density of the CCC and the percentage loading of SiC would be the most important factors determining the thermo-oxidative properties of CCC within the same group. Since the four PT-15 samples used different kinds of nanomaterials, they are not included in the subsequent discussion.

The following observations were made based on TGA result. For the DACC composites, the C/SiC material has a density of 2.1 g/cc outperformed the C/C material and all NCCCs with lower densities. For SiC CCCs, 10% SiC performed the best, 0% SiC the second, and 20% SiC the most unfavorable. On the other hand, 0% SiCp CCC had the least mass loss, 10% SiCp followed, and 20% SiCp was the poorest. Both 10% SiC and 0% SiCp had the highest density of 1.64 and 1.76 g/cc within its own group. Their relatively high thermo-oxidative resistance might be a result of their high density. Nevertheless, although 20% SiC had higher density than 0% SiC and 20% SiCp had higher density than 10% SiCp, their thermal stability was most unfavorable. This suggested that density was not the determining factor for this portion of the study. Since we had two or more variables in this experiment, more testing will be conducted before arriving at any firm conclusion.

5. SUMMARY AND CONCLUSIONS

Two resin systems (PT-15 cyanate ester and mesophase pitch monomer) and several types of nanoparticles (MMT nanoclay, POSS®, n-SiC, buckytubes, and CNFs) were selected for this study. The TEM analysis was used to characterize and screen candidates based on their degree of dispersion. Fourteen NCCC were fabricated. A C/C and a C/SiC type composites were fabricated by DACC. Heat-aging of the NCCCs was conducted using a vacuum furnace at 650°C for 50 and 100 hrs. and TGA under air up to 900°C and soaking for 5 hrs. at 650°C. Microstructural analyses were conducted on pre-test NCCCs.

The following conclusions were drawn from this study:

1. The TEM analysis has been demonstrated to be an effective and efficient tool to characterize and screen candidates based on their degree of dispersion.
2. MMT nanoclay and POSS® dispersed well in the PT-15 CE resin. TEM evidence of molecular dispersing of POSS® into PT-15 resin is presented.
3. Microstructure analyses of pre- and post-test NCCC specimens using SEM and optical microscope provided more fundamental understanding of material behavior.
4. The nanomodified CE CCC (PT15/30B, PT15/Im and PT15/POSS) are more thermo-oxidatively resistant than the baseline CCC (PT15).

5. With TGA for heat soaking in air environment, the DACC C/SiC composite exhibited the best performance and the AR mesophase pitch/SiC impregnated with Ceraset™ exhibited the most thermo-oxidative resistant NCCC. It was followed by the AR mesophase pitch/SiC NCCC. The nanomodified PT-15 CE NCCC is the poorest of the three NCCC groups.
6. The density of the NCCC and the percentage loading of SiC nanoparticles appear to be the most important factors determining the thermo-oxidative properties of NCCC within the same group.
7. Heat-aged studies of the remaining NCCCs using TGA in air and longer duration (1,000 hrs) should be conducted.

6. REFERENCES

1. PT-30 technical data sheet, Lonza Inc., Fair Lawn, NJ.
2. J. H. Koo, L. A. Pilato *et al.*, "Nanomodified Carbon/Carbon Composites for Intermediate Temperature: Processing and Characterization," AFOSR STTR Phase I Final Report submitted to AFOSR, Arlington, VA, Jan. 2004.
3. J. H. Koo, C. Pittman *et al.*, "Nanomodified Carbon/Carbon Composites for Intermediate Temperature: Processing and Characterization," *Proc. 35th International SAMPE Technical Conference*, SAMPE, Covina, CA (2003).
4. J. H. Koo, L. A. Pilato *et al.*, "Thermo-oxidative Studies of Nanomodified Carbon/Carbon Composites," *Proc. International SAMPE 2004 Symposium and Exhibition*, SAMPE, Covina, CA (2004).
5. K. Shivakumar, F. Abali, R. Sadler, J. McCoy, *Proc. International SAMPE 2000 Symposium and Exhibition*, SAMPE, Covina, CA (2000), p. 1005.
6. F. Abali, K. Shivakumar, N. Hamidi, and R. Sadler "An RTM Densification Method of Manufacturing Carbon-Carbon Composites Using PT-30 Resin," *Carbon* 41 (5), 893 (2003).
7. PT-15 technical data sheet, Lonza Inc., Fair Lawn, NJ.
8. M. L. Ramirez, *et al*, *Poly. Degrad. & Stab.* 78, 73 (2002).
9. US Patent No.: 6,309,703 B1, Oct. 30, 2001: P.G. Wapner, W.P. Hoffman, S. Jones, "Carbon and Ceramic Matrix Composites Fabricated by a Rapid Low-Cost Process Incorporating in-situ polymerization of Wetting Monomer."
10. AR Synthesized Mesophase Pitch technical data sheet, Mitsubishi Gas Chemical Company, Tokyo, Japan.
11. Cloisite® 30B technical data sheet, Southern Clay Products, Gonzales, TX.
12. J. H. Koo *et al.*, *Proc. International SAMPE 2002 Symposium and Exhibition*, SAMPE, Covina, CA (2002), p. 1085
13. J. H. Koo, H. Stretz, A. Bray, J. Weispfenning, Z.P Luo, and W. Wootan, *Proc. International SAMPE 2003 Symposium and Exhibition*, SAMPE, Covina, CA (2003), p. 1156-1170.
14. S. Ganguli, D. Dean, *et al*, *Polymer*, 44 1315, (2003).
15. J. W. Gilman *et al.*, *Chem. Mater.* 14, 3776 (2002).
16. J. W. Gilman *et al.*, *J. Poly Sci.*, Part B: Poly. Phy. 40, 2661 (2002).
17. S. Ganguli, D. Dean *et al.*, *Proc. International SAMPE 2003 Symposium and Exhibition*, SAMPE, Covina, CA (2003), p. 1132.
18. G.G. Tibbetts, *J. Crystal Growth* 1984; 66:632.

19. M. L. Lake, J-M. Ting. In *Carbon Materials for Advanced Technologies*, T.D. Burchell, Ed., Pergamon, Oxford: England (1999).
20. G. G. Tibbetts, M. L. Lake, K. L. Strong, and B. P. Rice, "A Review of the Fabrication and Properties of Vapor-Grown Carbon Nanofibers/Polymer Composites," *Composites Science and Technologies*, Vol. 67 (2007), pp. 1709-1718.
21. B. Maruyama and K. Alam, *SAMPE J.*, 38 (3), 59 (2002).
22. H. Ma *et al.*, "Processing, Structure, and Properties of Fibers from Polyester/Carbon Nanofiber Composites" manuscript.
23. J. H. Koo, D. Marchant *et al.*, *52nd JANNAN Propulsion Meeting*, Las Vegas, NV, May 10-14, 2004.
24. D. Zhu, *et al*, *J. Appl. Poly. Sci.* 87, 2063 (2003).
25. Trisilanolphenyl-POSS® (SO1458 POSS®) technical data sheet, Hybrid Plastics, Hattiesburg, MS.
26. Technical Bulletin No. 27 AEROSIL for Solvent-Free Epoxy Resin, AEORSIL Technical Service Dept., Degussa AG, D-63403 Hanau-Wolfgang, Germany.
27. AEROSIL® R805 technical data sheet, Degussa AG, D-63403 Hanau-Wolfgang, Germany.
28. AEROSIL® R202 technical data sheet Degussa AG, D-63403 Hanau-Wolfgang, Germany.
29. F. Yang, R. A. Yngard, G. L. Nelson, "Nanocomposites 2002," San Diego, CA, Sept 23-5, 2002.
30. J. H. Koo, *Polymer Nanocomposites: Processing, Characterization, and Applications*, McGraw-Hill, New York (2006).
31. Buckytubes technical data sheet, Carbon Nanotechnologies, Houston, TX.
32. Advanced SiC NanoPowder technical data sheet, Alpha Materials, Inc., St. Paul, MN.
33. Nano SiC Crystal Whiskers technical data sheet, Alpha Materials, Inc., St. Paul, MN.
34. Liao, F. *et al.*, *Applied Physics Letters*, **86**, 17913 (2005).
35. Vassen, R., and Stover, D., *J. Am Ceram. Soc.*, **82**, 2585-2895 (1999).
36. Neudeck, P. G., *J. Electronic Materials*, **24**, 283-288 (1995).
37. Burgemeister, E.A. *et al.*, *J. Applied Physics*, **50**, 5790 (1979).
38. Donaldson, K. Y. *et al.*, *J. Am. Ceram. Soc.*, **81**, 1583-1588 (1998).
39. Katoh *et al.*, *Ceramic Transactions*, **144**, 77 (2002).
40. Yang, Y.T. *et al.*, *Applied Physics Letters*, **78**, 162 (2001).
41. Rodgers, R. M. *et al.*, *Macromol. Materials and Eng.*, **290** (5), 423 (2005).
42. Yan, H., *J. Appl. Polym. Sci.*, **95**, 1246 (2005).
43. Xu, Y., Y. Tanaka, M. Murata, K. Kamihira, M. Yamazaki, and K. Yagi, "Effect of Reinforcement Nonuniformity on Effective Thermal Conductivity of Composite," Japan Institute of Metals, *Materials Transaction* (2005), **46** (8), pp. 1786-1789.
44. Li, L., and D .D. L. Chung, "Thermally Conductivity Polymer Matrix Composites Containing Both AIM Particles and SiC Whiskers," *Proc. 38th International SAMPE Symposium and Exhibition*, SAMPE, Covina, CA (1993), pp. 47-52.
45. J. H. Koo, S. Lao, J. Yong, G. Wissler, L. Pilato, and Z. P. Luo, "Cyanate Ester-Silicon Carbide Nanocomposites: Processing and Characterization," *Proc. International SAMPE 2006 Technical Conference*, SAMPE, Covina, CA (2006).

46. J. Cheng, S. Lao, J. Yong, J. H. Koo. P. Ferreira, L. Pilato, G. Wissler, and Z. P. Luo, "Cyanate Ester-Buckytubes Nanocomposites: Processing and Characterization," *Proc. International SAMPE 2007 Symposium and Exhibition*, SAMPE, Covina, CA (2007).
47. J. H. Koo, S. Lao, H. Jor, L. Pilato, J. Lee, G. Wissler, and Z. P. Luo, "Thermo-oxidative Studies of Nanomodified Carbon/Carbon Composites: Processing and Microstructural Characterization," *Proc. International SAMPE 2007 Symposium and Exhibition*, SAMPE, Covina, CA (2007).
48. J. H. Koo, S. Lao, H. Jor, L. Pilato, G. Wissler, J. Lee, and Z. P. Luo, "Thermo-oxidative Studies of Nanomodified Carbon/Carbon Composites for Intermediate Temperatures," *Proceedings of the 22nd Technical Conference of the American Society for Composites*, Seattle, WA (2007).
49. J. H. Koo, J. Lee, S. Lao, H. Jor, L. Pilato, G. Wissler, and Z. P. Luo, "Nanomodified Carbon/Carbon Composites: Further Thermo-oxidative Studies," *Proc. International SAMPE 2007 Technical Conference*, SAMPE, Covina, CA (2007).

ACKNOWLEDEMENTS

This work was sponsored by Air Force Office of Scientific Research (AFOSR) under AFOSR Contract No. FA9550-05-C-0028 (STTR Phase II) with Dr. Charles Y-C Lee as our Program Manager. The authors would like to thank Mr. W. Shih of Allcomp, Dr. S. Jones of SMJ Carbon Technology, Dr. C. Pittman of Mississippi State University, Mr. S.-J. Cheon of DACC in Korea, Dr. J. Lee of ADD in Korea, and Dr. Z.P. Luo of Texas A&M University for supporting the program. The authors would also like to thank our students at the University of Texas at Austin especially S. Lao, J. Cheng, H. Jor, and J. Yong for conducting the experiments.